EXPERIMENTAL AND THEORETICAL STUDIES ON THE MECHANO-OPTICAL AND ENERGY BEHAVIOR OF THERMOPLASTIC POLYURETHANEUREAS

by

Sezen Cürgül

A Thesis Submitted to the
Graduate School of Engineering
in Partial Fulfillment of the Requirements for
the Degree of

Master of Science

in

Mechanical Engineering

Koç University

June, 2004

Koç University

Graduate School of Sciences and Engineering

This is to certify that I have examined this copy of a master's thesis by

Sezen Cürgül

and have found that it is complete and satisfactory in all respects,
and that any and all revisions required by the final
examining committee have been made.

Committee Members:

Prof. Burak Erman (Advisor)

Assist. Prof. Murat Sözer

Assist. Prof. Levent Demirel

Date: June 21, 2004

To my family

ABSTRACT

In the experimental part of this thesis, effect of composition on the mechano-optical properties of thermoplastic polyurethaneureas was investigated by selectively varying the type and content of soft and hard segments. Real time stress-strain-birefringence experiments were coupled with the off-line Wide Angle X-Ray Scattering measurements. These experiments together with Differential Scanning Calorimetry measurements revealed that soft segments and chain extenders play dominant roles on the chemical structures of the polyurethaneureas. In general, samples with lower fraction of hard segment exhibited higher crystallizability than their high hard segment counterparts. Long term holding of poly(ethylene oxide) samples in stretched state was found to increase crystallinity. The strain rate is found to have a considerable effect on the crystallization behavior of poly(ethylene oxide) based samples. From birefringence-true stress data, linear and non-linear stress optical behavior were investigated. It was observed that the span of the initial linear stress optical region varied primarily with composition (slope ranging from 0.1 to 2.2 GPa^{-1}) and secondarily with the deformation rate. Hysteresis experiments showed that there is a considerable loss of energy in cyclic loading of these materials and hysteresis increases as the chain extender is changed from 1,6-diaminohexane to ethylene diamine. In the theoretical part of the thesis, hysteretic energy behavior of the same materials was investigated. The amount of energy that is permanently lost and the amount of energy that may be recoverable in hysteresis is distinguished and a model to calculate these energies has been proposed.

ACKNOWLEDGMENTS

First I would like to thank my advisor Professor Burak Erman. Without his help and support, I would not have been able to finish this thesis. I find myself very lucky to be a student of him and that I was able to take advantage of his deep knowledge and experience. His advice both professional and personal is invaluable to me. Next, I would like to thank my co-advisor Professor İskender Yılgör and Emel Yılgör together with the polymer group at Koc University for supplying the materials used in this study. I greatly appreciate their help and advice. I would also like to thank Professor Miko Çakmak and his research group members who helped me during my studies at the University of Akron. I am grateful for his time commitment, his intriguing questions and his advice. I also want to thank to the members of my committee, Assist. Prof. Murat Sözer and Assist. Prof. Levent Demirel for giving time and for their valuable comments.

I am also indebted to the members of my family whose contributions and supports can not be assessed enough. Mom, Dad and my dear brother, thanks so much for your love and support.

This kind of work is never completed by a single individual but by someone who receives the contribution of others. I am grateful to everyone whom I cannot name here.

TABLE OF CONTENTS

LIST OF TABLES

LIST OF FIGURES

NOMENCLATURE

TPUU	Thermoplastic Polyurethaneurea
PEUU	Polyether Polyurethaneurea
WAXS	Wide Angle X-ray Scattering
SAXS	Small Angle X-ray Scattering
DSC	Differential Scanning Calorimetry
HMDI	Bis(4-isocyanatocyclohexyl)methane
NDI	Naphthalene -1.5- Diisocyanate
MDI	Diphenylmethane -4.4'- Diisocyanate
PTMO	Poly(tetramethylene oxide) Glycol
PEO	Poly(ethylene oxide)
ED	Ethylene Diamine
HMDA	1,6-Diaminohexane
DMF	Dimethylformamide
Tg	Glass Transition Temperature
Tc	Crystallization Temperature
Tm	Melting Temperature
HS	Hard Segment Amount By Weight
TS	True Stress
σ	Stress
t	Time

Chapter 1

INTRODUCTION

Polyurethane chemistry opened the way to a new class of high performance materials such as coatings, adhesives, elastomers, fibres and foams. Based on a simple polyaddition reaction, the polyurethanes proved to be very versatile polymers. Materials with tailor-made properties can be produced from the broad variety of the chemicals used. Today, thermoplastic polyurethanes play an important role within the rapidly growing family of thermoplastic elastomers.

The original discovery leading to the world-wide interest in all classes of urethanes was made by Otto Bayer and his coworkers of I.G. Farbenindustrie at Leverkusen, Germany (now Bayer AG) in 1937 as a competitive response to the work by Carothers of DuPont, USA, on the polyamides or nylons. Subsequently, the elastomer properties of polyurethanes were recognized by DuPont and by ICI. By the 1940's polyurethanes were produced on an industrial scale. This first so-called "I-rubber", however, had very poor properties. To overcome the deficiencies which were supposed to stem from a non-regular elastomeric network, a polyurethane elastomer was synthesized which consisted of linear polyesters and 2-nitro-4,4'-diisocyanate-biphenyl. In a second step, the nitro groups were to be reduced to form azo linkages. Surprisingly, this later step proved to be unnecessary, because the original polymer, which was chain extended by water, already showed interesting elastomeric behavior. A similar result was obtained when the nitrodiisocyanate was replaced by naphthalene-1.5-diisocyancate. These unexpected results were explained in terms of the following reaction sequence: First the strictly linear hydroxyl terminated polyester reacts with an excess diisocyanate to form a diisocyanate prepolymer. This prepolymer is subsequently chain extended by water, leading to urea linkages. The urea linkages react with further diisocyanate to build an elastomeric network. Chain extension by short chain diols proved to be the breakthrough to polyurethane elastomers, which were tradenamed by Bayer as Vulkollan®. In the USA,

Chemigum SL® was an early Vulkollan type polyester urethane elastomer which was developed by Seeger et al. of Goodyear Tire and Rubber Co. DuPont marketed Adiprene® a polyether urethane.

Early polyurethane elastomers consisted of basically three components: i) A polyester or polyether macrodiol. ii) A chain extender such as water, a short chain diol, or a diamine. iii) A bulky diisocyanate, e.g. naphthalene-1.5-diisocyanate (NDI). However, these polyurethane elastomers were not yet real thermoplastic polyurethane elastomers in the proper sense of the term, since their melting temperature was higher than the decomposition temperature of the urethane linkages.

Great progress was achieved when NDI was replaced by diphenylmethane-4.4'-diisocyanate (MDI) in the above mentioned three component system. Schollenberger of B.F.Goodrich described a thermoplastic polyurethane in 1955. Somewhat earlier DuPont announced a Spandex fiber called Lycra®, a polyurethane based on MDI. By the early 1960's Goodrich marketed Estane®, Mobay Texin®, Upjohn Pellethane® in the USA. Bayer and Elastogran marketed Desmopan® and Elastollan® respectively in Europe. In the following years much effort was spent to elucidate the nature of bonding, structure-property-relationship, resulting in the synthesis of many specialized forms, and in particular plastics and rubbers in solid and cellular form, surface coatings, adhesives, and fibres. The range of products is shown in Figure 1.1, which illustrates the molecular structure features used to produce such diverse polymer foams, some fibre- or film-forming, some thermoplastic or thermosetting and others elastomeric.

An urethane elastomer can be regarded as a linear block copolymer of the type shown in Figure 1.2. This segmented polymer structure can vary its properties over a very wide range of strength and stiffness by modification of its three basic building blocks: the polyol, diisocyanate and chain extender. The polyol constitutes the soft segment and consists of the long flexible polyether or polyester chains which interconnect two hard segments. Diisocyanate together with the chain extender make up the hard segment.

At room temperature, the low melting soft segments are incompatible with the polar high melting hard segments, which leads to a microphase separation. A part of the driving mechanism for phase separation is the development of crystallinity of the hard segments. Upon heating above the melting temperature of the hard segments, the polymer forms a

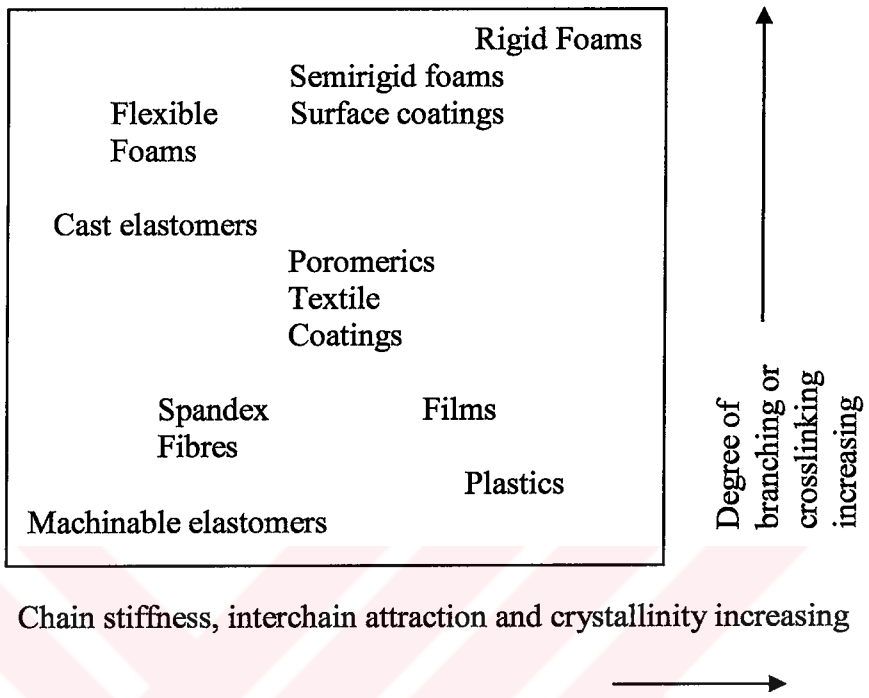

Figure 1.1: Structure - Property relationships in polyurethanes.

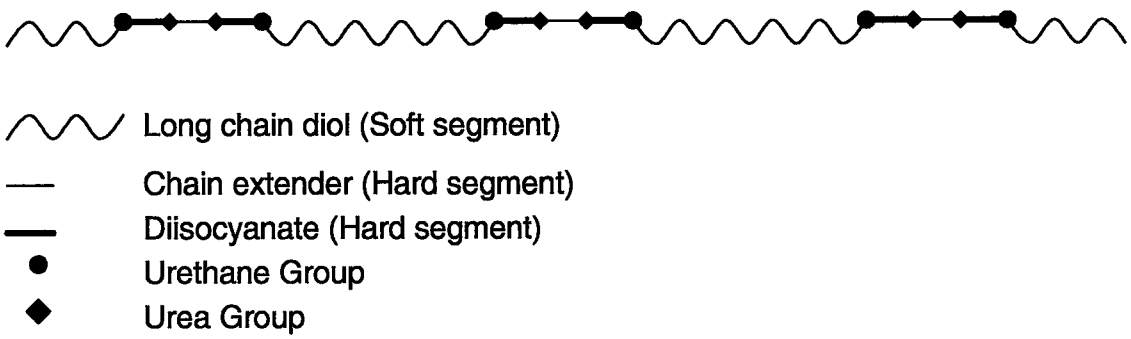

Figure 1.2: Schematic representation of a thermoplastic polyurethaneurea composed of a diisocyanate, long chain diol and chain extender.

homogeneous viscous melt which can be processed by thermoplastic techniques such as injection molding, extrusion, blow molding, etc. Subsequent cooling leads again to segregation of hard and soft segments.

Usually, the soft segments form an elastomer matrix which accounts for the reversibly elastic properties of thermoplastic polyurethane, with the hard segments acting as multifunctional tie points functioning both as physical crosslinks and reinforcing fillers. However these crosslinks can be reversibly overcome by heat or solvation. Then by cooling or on desolvation a thermoplastic polyurethane network is reformed.

As discussed above, thermoplastic polyurethaneureas (TPUUs) show a complex morphological behavior that strongly depends on their chemical compositions and backbone structures. In this study, a new series of TPUUs were synthesized and information regarding their mechano-optical properties was acquired using a uniaxial stretching apparatus in combination with offline Wide Angle X-Ray Scattering (WAXS) studies. Also the hysteretic energy behavior of the same materials was investigated. The amount of energy that is permanently lost and the amount of energy that may be recoverable in hysteresis are distinguished and a model to calculate these energies has been proposed. Chapter 2 gives the literature review of the above subjects. In Chapter 3, the structure of materials, experimental procedures and instrumentation are explained. Derivation of the viscoelastic work function is accomplished in Chapter 4. Chapter 5 gives the important results acquired from the experimental studies. Energy calculations related to the viscoelastic work function can be found in Chapter 6. Finally, conclusion is given in Chapter 7.

Chapter 2

LITERATURE SURVEY

Being a linear block copolymer, the polyurethaneureas usually contain three main components: The polyol which is also called the soft segment, the diisocyanate and the chain extender which are together called the hard segment. Depending on the concentration and type of these units, TPUUs can have very different properties including high strength, hardness, high elongation to break and high modulus of elasticity than many other elastomers. The main mechanism underlying these unique properties is the phase separation of the hard and soft segments which have been the subject of many studies previously.

Cooper and Tobolsky [1] were first to propose a phase separated domain morphology for elastomeric polyurethanes in 1966. They showed that the viscoelastic properties of polyurethanes were similar to that of known block copolymers and the results indicated phase separation and reinforcement. From that time on, the unique properties of polyurethanes have been associated with microphase separation of the hard and soft segments, in which soft segment units giving the elastomeric behavior while hard segments provide physical cross-linking. Thermodynamic driving forces and the kinetic paths that have been followed during processing are the two main factors that determine the amount and type of microphase separation. Also the degree of incompatibility between the hard and soft segments determines the amount of microphase separation which has a profound effect on the polymer's ultimate properties.

The microstructure of these materials was first investigated using X-ray diffraction by Clough and co-workers [2, 3] at the U.S. Army Materials Research Laboratory (Natick, Mass.). Bonart [4] studied polyurethane morphology by Small-Angle-X-Ray Scattering (SAXS) and reported preferred orientation of the periodic microphase structure as a result of tensile stretching. He proposed that during the initial elongation, the soft segments, depending on their accidental position in the unstretched starting material, are stretched to different extents and are therefore also placed under different loads. This entails locally

varying tensile forces, and thus locally varying torques, at the ranges of cross-linking, which causes the transverse positioning of the hard segments in cases of elongations of up to 200 or 300 %. On the other hand, the elongation crystallization begins only in the immediate vicinity of the fully stretched soft segments due to the sufficient lowering of entropy there. Consequently, only the fully stretched and fully oriented chain pieces are active as nuclei for the elongation crystallization, so that all soft segment crystallites obtained are fully oriented from the very beginning. At the same time, the maximally loaded chain pieces of the soft segments form, with the ranges of cross-linking located between them, what are called force strands, which follow the molecular chains only section-wise and which oppose any further lengthening. With increasing macroscopic elongation of the material, the force strands present in each individual case therefore break, because the growing shear forces within the ranges of cross-linking lead to sliding processes between the hard segments. At the same time, new force strands are formed, with the hard segments more turning themselves with their longitudinal axes into the direction of elongation. He also suggested enhanced phase separation by longer average segment lengths and observed that polyether based polyurethanes experience greater phase separation than polyester based polyurethanes [4].

Many other models have been suggested to describe the domain structure of phase separated polyurethanes based upon X-ray and other indirect viscoelastic measurements and thermal analysis [5, 6, 7]. Estes et al. [6] proposed a morphology in which both phases are represented as being continuous and interpenetrating, yet not completely phase separated. Bonart [7] suggested a three dimensional model to account for the high degree of interurethane hydrogen bonding measured experimentally. Bonart's model leads to the development of a large scale structural model based on a lamellar arrangement of the hard segments. Wilkes [8] observed two types of spherulitic structures in polyurethanes, and hard segments were suggested to orient either radially or tangentially in the spherulites in order to explain the different types of optical symmetry observed.

The incorporation of urea linkages in the polyurethane hard segment has a profound effect on the phase separation and domain structure of polyether polyurethaneureas (PEUUs). This is due to the high polarity difference between hard and soft segments and the likely development of a three dimensional hydrogen bonding network as explained by Sung et al. [9] who studied the mechanical properties of polyurethanes in order to demonstrate the

consequences of phase segregation and domain structures. In a series of papers by Sung et al., [9, 10, 11] the properties of segmented PEUUs based on 2,4-tolyl diisocyanate, ethylene-diamine (ED), and poly(tetramethylene oxide) (PTMO) have been described. In general, considerable improvement in the extent of microphase separation was found in the PEUU's extended with ED compared to all polyurethane systems chain extended with butanediol. This was suggested by a much lower glass transition temperature (Tg) of the soft segment phase and a much higher Tg of the hard segment domains in PEUU's. The interphase between the hard domain and soft matrix was suggested to be quiet sharp as most of the urethane carbonyls were non-hydrogen bonded. In addition, mechanical properties indicated that at the same hard segment content (30%), the hard domains in the PTMO with a molecular weight of 1000 sample were more interconnected than the hard segment domains in the PTMO with a molecular weight of 2000 sample and that the soft segment phase of the former contained more solubilized hard segment. Wilkes et al. [12] investigated the morphology of Sung's PEUU's using SAXS and found a consistent interpretation of his data with the results obtained by using mechanical and thermal tests. One important observation was that one-dimensional correlation function displayed periodicity. This suggested that the two-phase microstructure can be described as alternating layers of soft and hard segments whose spacing was given by the calculated periodicity. Wilkes also suggested that the diamine chain extender promoted better phase separation since the thickness of the interphase between the domains in the PEUU's was somewhat less than that of conventional polyurethanes using butanediol as the chain extender.

In addition to soft segment, hard segment also plays a major role in microphase separation. The amine cured polyurethanes show a greater propensity toward microphase segregation than their diol-cured counterparts, presumably because of the large number of possible hydrogen bonds between hard segment chemical groups [9, 10, 11, 12]. Cooper et al. [13] observed that the mechanical properties depend primarily on hard segment content and especially on the concentration of urea linkages. This suggests an improvement of hard domain cohesion and an enhanced filler effect through the formation of three dimensional urea hydrogen bonds in the PEUUs. He proposed a transition of morphology from interconnecting hard and soft segment domains to isolated hard segment domains in a soft segment matrix upon decreasing the hard segment content. He concluded that small differences in

the orientation behavior of the hydrogen bonded and nonbonded urethane units at the hard domain interface could lead to the slightly different morphology of each sample. Studies of segmental orientation of hydrogen bonded PEUUs revealed a marked change in orientation behavior as the MDI content increased from 24 to 28 wt % [14] suggesting a change in morphology from isolated to interconnected hard segment domains. Transverse orientation at low strains was indicated by an orientation inversion in those polyurethanes with partially crystalline hard segments. Ishihara et al. [15, 16] observed the presence of spherulitic crystalline texture in segmented PEUUs and proposed a deformation mechanism whereby this structure disintegrated into a paracrystalline fiber texture upon elongation of the sample. The model is consistent with the observation of the initial hard segment transverse orientation found by infrared dichroism. In some studies, [17, 18], it was found that increasing the segmental length of hard segments can increase the amount of phase separation. In another study [19], it was stated that increasing the hard segment amount results in larger hard segment domain sizes and higher hard segment domain concentrations in the soft segment matrix.

Most TPUUs are highly elastomeric and can be elongated to very high stretch ratios. Releasing the applied strain results in quick and complete recovery of the original shape. This extraordinary behavior makes these materials suitable for many applications involving cyclic loading. Cooper and Wang [13] studied hysteresis in MDI-ED polyurethanes with different molecular weights of the soft segment polytetramethylene ether glycol (PTMEG). They found that samples with high hard-segment content had high hysteresis, which they attributed to hard domain interconnectivity, and plastic deformation in the hard domains which occurred at low strains due to the high degree-of-order in those domains. Samples with lower hard segment contents or higher soft segment molecular weight had a lower hysteresis because the hard domains were dispersed throughout the soft segment matrix. Studies by Allegrazza [20] with non hydrogen bonded polyurethanes, point out the critical role played by the hard segment domains to act as physical crosslinks and to reduce mechanical hysteresis. Lower hysteresis has been found in systems which were less prone to strain-induced crystallization [21, 22, 23, 24]. Such crystallization was minimized by introducing non-symmetrical soft segments such as copolymers or polyfunctional soft segments. Also, polymer blends or broad molecular weight distributions of soft and/or hard segments

may be used to reduce the high degree of domain ordering which favors strain-induced crystallization. Infrared orientational studies of hysteresis [25] showed that plastic deformation occurs predominantly in hydrogen bonded hard segment domains due to the disruption of the structure in the hard segment aggregates and soft and hard segments residing in the soft phase show substantial recovery upon unloading. According to SAXS data taken during the study of Desper et al. [26], the hard segment phase breaks up into smaller chunks, compromising physical cross-linking effect. Such behavior is attributed to a higher level of mechanical hysteresis. The second elongation was found to produce a higher stress than the stress reached in the previous cycle [55]. It was then concluded that hard segments break upon elongation and reconstruct partially upon recovery. Some studies [14, 15, 16, 27, 28] differentiated between hysteresis at small and large strains; indicating that low mechanical hysteresis occurred at small strains where the morphology of the polymer was not permanently disrupted. Low strain level hysteresis experiments [14] show that loading and unloading is nearly a reversible process. As the elongation is increased, however, the original crystallites are broken up and the segments orient positively. Orientation of the crystalline hard segments thus occurs in two steps. First the positive orientation of the crystalline region itself, followed by disruption of the region and increasing positive orientation of the segments. An increase in mechanical hysteresis was attributed to morphological changes and to processes which lead to permanent deformation. Abouzahr et al. [24] suggested that hysteresis occurred due to different mechanisms at different strains. At strains below 50%, energy dissipation was associated with nonaffine deformation and orientation of the hard segment domains. Between 50 and 500% strains, disruption of hard domains and hard segment backbone chain alignment occurred, whereas at higher extensions, hysteresis had little dependence on extension because the domains were already disrupted. They considered that hysteresis here arose from chain slippage and the different viscoelastic responses of the hard and soft segments. With high hard segment content, they found that domain disruption occurred at low elongation and hence the first of these mechanisms was not observed. At low hard segment content, they argued that the hard segment in their system was largely solubilized in the soft domains and the lack of crosslinks allowed flow and high energy dissipation during stress cycling. In another study [29], it was concluded that at low strain, internal friction was a contributing factor to hysteresis. The softer materials with the

higher molecular weight soft segments showed soft segment crystallization and the increase in hysteresis with strain in these materials may have resulted from increasing amounts of strain-induced crystallization. At low strains, interconnectivity of the hard domains may have resulted in slightly higher hysteresis in the lower molecular weight soft segment materials leading to increased internal friction. The increase in hysteresis with strain in the harder materials was related to the deformability of the hard domains.

Phase separation and relaxation kinetics have also been studied with Differential Scanning Calorimetry (DSC) techniques [30, 31, 32]. Helgee et al. [32] investigated the effect of soft segment length and chain extender structure on the phase separation behavior of polyurethaneureas and found that diamines with odd numbers of methylene groups effectively restrict the thermal molecular motion by the phase mixing of the hard and soft segments compared to diamines with even numbers of methylene groups. It was also shown that [33] the Tg of the soft phase decreases with increasing hard segment content which is in contrast to increased hard segment mixing in the soft phase, but can be rationalized by taking into consideration soft segment crystallinity. Cooper et al. [13] found that presence of a PTMO melting endotherm in PTMO samples with molecular weight 2000 g/mol and this peak was correlated with improved phase separation than lower molecular weight PTMO samples. He also suggested that soft segment crystallization proceeds more completely under a slower cooling rate. It is also noted that both quenching and slow cooling enhance soft segment crystallization. The main conclusion that was drawn by the DSC studies of Wilkes et al. [8] is that for polyurethanes made from different prepolymers or different chain extenders, but the same diisocyanate, the relative extent of formation of hydrogen bonded urethane domains is not a direct function of weight percent urethane. He also suggested that under thermal treatment, a well ordered structure develops in the interpenetrating hard domain and soft segment regions.

Some materials, including TPUUs, exhibit elastic action upon loading if loading is rapid enough. Then a slow and continuous increase of strain at a decreasing rate is observed. When the stress is removed, a continuously decreasing strain follows an initial elastic recovery. Such materials are significantly influenced by the rate of straining and stressing; i.e., for example, the longer the time to reach the final value of stress at a constant rate of stressing, the larger the corresponding strain. These materials are called viscoelastic. The time

dependent behavior of viscoelastic materials must be expressed by a constitutive equation which includes time as a variable in addition to the stress and strain variables [34]. When a viscoelastic material is deformed by the application of a force, some of the mechanical work required is stored in the material and the remainder is dissipated as heat. This energy dissipation or hysteresis in the material results from several different mechanisms which are dependent on the type of the material and the experimental conditions. The major sources of hysteresis can be listed as viscoelasticity, crystallization, breakdown of hydrogen bonds, changes in network configurations and changes in network structure [35]. The energy lost may be dissipated as heat, consumed by morphological changes or go unmeasured during the time scale of the experiment. Consequently, some part of the energy may be recoverable with time due to viscoelastic behavior of the TPUUs and some other part is permanently lost.

Since it is important to distinguish between these two parts of the energy, modeling the hysteresis of elastomeric materials have been the subject of many studies. Several studies propose to model hysteresis of elastomeric materials by introducing viscosity [36] or damage [37, 38] or both of them. DeSimone et al. [38] studied stress softening phenomenon from the point of damage mechanics. Stress softening is a typical phenomenon observable for many materials during cyclic tension tests; when a given specimen is subjected to a load-unload-reload cycle, the stress accompanying a given stretch is always smaller during reloading than in the virgin loading path. If permanent set effects are negligible, stress softening can be described as a decay of elastic stiffness as the maximum strain (or stress) ever experienced by the material increases. Stress softening is particularly evident for specimens of rubber where it is known as Mullins effect. It has received considerable attention, not only in the early days of its discovery [39], and the pioneering experimental and theoretical work of Mullins [40, 41], but also in recent times. More recently, interest towards the development of simpler models, aiming at a conceptual understanding of the essentials of the phenomenon, has emerged. Models using a single scalar damage variable, either energy based [36], or based on the notion of maximum strain experienced by the material in its deformation history [41], have been proposed and compared with data from uniaxial experiments. However the study of the micro-structure of elastomeric materials [42, 43] allows one to highlight the existence of a time dependent hysteresis and then a nonviscous internal friction. Several

models for the representation of hysteresis loops have been proposed in small deformations [44, 45], and their common expression for thermodynamics potential has the general form function of states variables α and β which represent the internal sliding and the inelastic deformation of the material due to friction, respectively. Cantournet et al. [46] concluded that the introduction of viscosity or damage is not necessary to model hysteresis and stress softening (Mullins effect) of elastomeric materials.

Chapter 3

MATERIALS AND EXPERIMENTS

3.1 Objective

As it can be seen from the literature survey, each TPUU has its own properties and its structure-property relationship must be determined separately. Experimental methods like the standard tensile test, x-ray studies like WAXS and SAXS, DSC, Fourier Transform-Infrared Spectroscopy (FTIR), Atomic Force Microscopy (AFM) and Scanning Electron Microscopy (SEM) are some of the methods which are used to determine this relationship.

The objective of the experimental work in this study is to acquire information regarding the mechano-optical properties of a series of TPUUs which were synthesized for this study. For this purpose, an automated tensile uniaxial stretching apparatus in combination with offline WAXS studies were used. The thermal behavior of the same materials was investigated by DSC. What makes this study different from other studies is that the polyurethanes under consideration are unique and they are high strength TPUU's which can function under heavy loading conditions (up to 40 MPa). Another fact is that the uniaxial stretching machine is capable of measuring true stress-strain values online together with birefringence which allows a unique look at the mechano-optical behavior.

3.2 Materials

Bis(4-isocyanatocyclohexyl)methane (HMDI) with a purity higher than 99.5% was obtained from Bayer AG, Leverkusen, Germany. PTMO with a number average molecular weight (Mn) of 2040 g/mol was received from Du Pont, USA. α,ϖ-Amine terminated poly(ethylene oxide) oligomer (PEO) (Jeffamine ED2003) (Mn=1975 g/mole, from end group titration) was kindly provided by Huntsman Corp. Reagent grade ED, 1,6-diaminohexane (HMDA), dimethylformamide (DMF) and isopropanol (IPA) were obtained from Aldrich. Dibutyltin dilaurate (DBTDL) catalyst was obtained from Witco. Water contents of PTMO, PEO and DMF were determined by Karl Fisher titration and were found to be less than 300 ppm.

All chemicals and solvents were used as received.

3.3 Polymer Synthesis

A two-step procedure was followed during the preparation of segmented TPUU copolymers. First step was the formation of an isocyanate terminated prepolymer, followed by the chain extension to form high molecular weight copolymers. PTMO based prepolymers were prepared in a four-neck, flat bottomed 1L pyrex reaction kettle fitted with an overhead stirrer, addition funnel, thermometer and dry nitrogen inlet. Kettle was charged with calculated amounts of HMDI and PTMO, heated up to 80°C and stirred. Reaction was started by the addition of 0.005 g of DBTDL catalyst in 1 ml of toluene. The reaction was followed by FTIR spectroscopy, monitoring the disappearance of sharp isocyanate peak at 2270 cm^{-1} and broad hydroxyl peak at 3400 cm^{-1} and formation of strong urethane (C=O) and (N–H) peaks at 1750 and 3300 cm^{-1} respectively, using a Nicolet Impact 400D spectrometer. Prepolymer formation was generally completed in two hours. Isocyanate content of the prepolymer was determined. The prepolymer was dissolved in 250 g of DMF and the solution was cooled down to room temperature before chain extension.

PEO based prepolymers were also prepared in a four-neck, 1L pyrex reaction flask fitted with an overhead stirrer, addition funnel, thermometer and dry nitrogen inlet. HMDI was weighed into the kettle and dissolved in IPA. Calculated amount of PEO was separately dissolved in IPA and introduced into an addition funnel. Prepolymer was prepared by the dropwise addition of PEO into the reactor at room temperature. Completion of reaction was confirmed by FTIR spectroscopy. For chain extension, calculated amounts of diamine chain extenders (ED, HMDA) were dissolved in IPA, introduced into the addition funnel and added into the prepolymer solution at room temperature under strong agitation. The reactions were followed by FTIR spectroscopy, monitoring the disappearance of sharp isocyanate peak at 2270 cm^{-1}. Towards the end of the chain extension process as the viscosity of the reaction medium increased, reaction mixture was diluted by the addition of IPA.

Table 3.1 provides the chemical compositions and corresponding codes of the segmented polyurethaneurea and polyurea copolymers prepared and investigated in this study.

The actual hard segment content in PE-HMDA-20 and PE-ED-20 is 22.7%. As shown in Table 3.1, eight different samples falling into four groups according to their chemical

Table 3.1: Polymer codes and compositions of the TPUUs

Group no	**Code**	**Polyol/Diisocyanate/Chain Extender**
1	PT-HMDA-20	PTMO/HMDI/HMDA
1	PT-HMDA-30	PTMO/HMDI/HMDA
2	PT-ED-20	PTMO/HMDI/ED
2	PT-ED-30	PTMO/HMDI/ED
3	PE-HMDA-20	PEO/HMDI/HMDA
3	PE-HMDA-30	PEO/HMDI/HMDA
4	PE-ED-20	PEO/HMDI/ED
4	PE-ED-30	PEO/HMDI/ED

structures were prepared and characterized. The first column gives the group number. Second column provides the coding, which works as follows: the first two letters indicate the soft segment type (PT=PTMO and PE=PEO), next two or four letter code denotes the chain extender, two digit number that follows show the weight percent of the hard segment in the copolymer. In the third column, individual components that constitute the chemical composition of the copolymers are given in the following order: polyol/diisocyanate/chain extender. All copolymers were prepared from the same diisocyanate, HMDI. The chain extender is either HMDA or ED.

The samples listed in Table 3.1 all have the same hard segment block, HMDI. They are designed to have different combinations of the soft segments and chain extenders. We consider four groups, each with different combinations of the soft segments and chain extenders: (i) Samples in the first group have PTMO as their soft segment and HMDA as the chain extender. (ii) Group 2 samples have PTMO as the soft segment and ED as the chain extender. (iii) Samples in group 3 have PE as the soft segment and HMDA as the chain extender. (iv) Samples in the fourth group have PE as the soft segment and ED as the chain extender.

Detailed chemical structures of the four groups of polymers shown in Table 3.1 are presented in Table 3.2. The second column denotes the nomenclature adopted in this study.

In Table 3.2, R_1 indicates a dicyclohexylmethane radical. R_2 is PEO whose structure

Table 3.2: Chemical structure of the materials

Group	Code	Composition
1	PT-HMDA	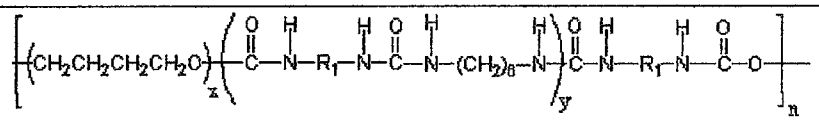
2	PT-ED	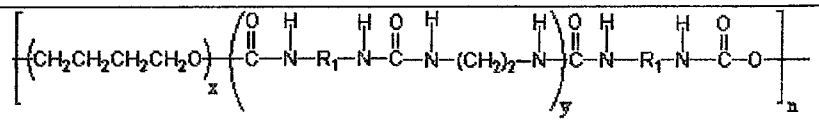
3	PE-HMDA	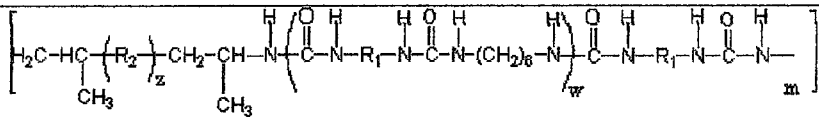
4	PE-ED	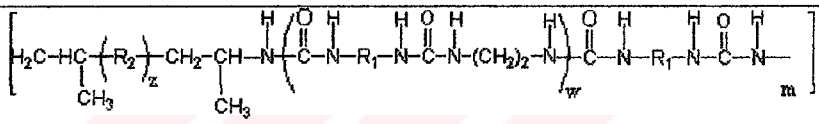

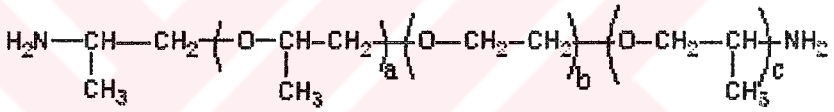

Figure 3.1: Structure of PEO

can be seen in Figure 3.1, where b is approximately 39 and a+c is 6.

The number of repeat units (x) is around 28 in all PTMO based materials. The number of repeat units (z) in the soft segment was about 39 for all PE based materials. The number (y) denotes the number of repeat units which is composed of HMDI and the chain extender for the PTMO based samples. It is equal to 1.6 for high hard segment content sample in the first group and 0.6 for the low hard segment content one in the same group. For the second group, (y) is equal to 1.9 for the sample with HS=30% and 0.7 for the sample with HS=20%. Likewise (w) is the number of repeat units for the PEO based samples and is equal to 1.6 for the high hard segment content material in the third group and equal to 0.6 for the low hard segment content material in the same group. For the last group samples, (w) is equal to 1.9 for the sample with HS=30% and to 0.7 for the sample with HS=20%. The whole unit for the PTMO based materials repeats n times, which is equal to 25 for

PT-HMDA-30, 30 for PT-HMDA-20, 20 for PT-ED-30 and 25 for PT-ED-20. For the PEO based materials the whole unit repeats m times, which is equal to 30 for PE-HMDA-30, 40 for PE-HMDA-20, 25 for PE-ED-30 and 30 for PE-ED-20.

3.4 Sample Preparation

Polymer films were prepared in Teflon molds by solvent casting. The solvent was first evaporated at room temperature overnight and then at 60°C in an air oven and finally in a vacuum oven at 60°C until constant weight was reached. The samples were kept in sealed polyethylene bags until testing.

3.5 Instrumentation

3.5.1 Instrumentation for Uniaxial Stretching

Simultaneous measurements of true stress-true strain-birefringence were made at room temperature with the help of highly automated instrument which can be seen in Figure 3.2. The instrument was built and used at the Polymer Engineering Department of University of Akron, OH.

The stretching machine is designed to stretch both top and bottom cross head in opposing directions in order to maintain mid point observation point stationary. The spectral birefringence is measured from this mid point using the automated system. The details of the instrumentation have been documented extensively before [47]. Online-birefringence is essentially based on the method described by Posthuma de Boer et al. [48]. The characteristic of this method is using white light as light source to get the order number of retardation automatically. When we use the white light, representative light intensities through sample and a pair of cross polarizer is shown in Eqs. 3.1 and 3.2.

$$I^{\perp} = \frac{I_0}{2} e^{-2\alpha} \sin^2\left(\frac{\pi \Delta n d}{\lambda}\right) \tag{3.1}$$

$$I^{\parallel} = \frac{I_0}{2} e^{-2\alpha} \cos^2\left(\frac{\pi \Delta n d}{\lambda}\right) \tag{3.2}$$

Here I is light intensity. The term $e^{-2\alpha}$ accounts for attenuation of light caused by

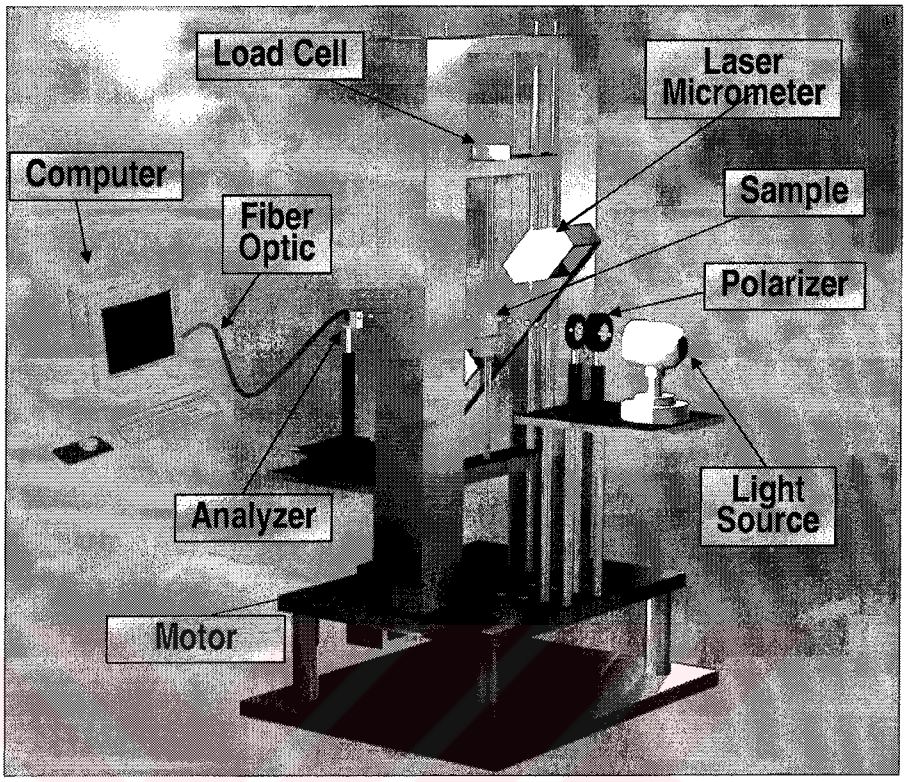

Figure 3.2: The automated uniaxial tensile stretching machine.

scattering from the sample. Δn is birefringence and d is thickness of the sample. λ is the wavelength of the light.

After detecting the light intensity of each component, the computer calculates normalization value of light intensity to erase the attenuation factor Eq. 3.3:

$$N^{\perp} = \frac{I^{\perp}}{I^{\parallel} + I\perp} = \sin^2\left(\frac{\pi \Delta n d}{\lambda}\right) \tag{3.3}$$

The difference in period varied with the retardation. When t_{pi} is put to each peak of $\sin^2(\varpi t)$, the period can be expressed as in Eq.3.4

$$\frac{\pi}{\varpi} = |t_{pi+2} - t_{pi}| \approx |2\,(t_{pi+1} - t_{pi})| \tag{3.4}$$

$$R = \Delta n d \approx \frac{\lambda_{pi+1}\lambda_{pi}}{2\,|\lambda_{pi+1} - \lambda_{pi}|} \tag{3.5}$$

As t in $\sin^2(\varpi t)$ corresponds to $\frac{1}{\lambda}$ in $\sin\left(2\frac{\pi\Delta nd}{\lambda}\right)$ and ϖ in $\sin^2(\varpi t)$ correponds to $\pi\Delta nd$ in $\sin^2\left(\frac{\pi\Delta nd}{\lambda}\right)$, respectively, Eq.3.5 is acquired which is the relation between retardation and wavelength in the peak of the normalized light intensity. Here R is the retardation of the sample.

This technique is automated to obtain real time retardation measurements at about 3-5 Hz at 633 nm wavelength. Representative dispersion curves are also automatically determined by

$$R \approx R_0 + \frac{a}{\lambda^2} \tag{3.6}$$

in the range of 460-650 nm. Here R_0 (in nm) is the retardation at the infinite wavelength which is dependent on the degree of molecular orientation, and a is a material constant.

In order to determine the birefringence, the thickness needs to be measured at the same time and at the same location where the birefringence is measured. This is accomplished using a laser micrometer mounted at an oblique angle that ensures the width measurement of the sample at the same position as the retardation measurement was made. This allows continuous width monitoring during stretching. The transverse isotropy assumption is made (Eq. 3.7), $\varepsilon_{TransverseDirection} = \varepsilon_{NormalDirection}$, in order to determine the time variation of local thickness as well as true stress and true strain. Another assumption is that the polymer under consideration is incompressible. This assumption (Eq.3.8) is used to calculate the true strain.

$$\frac{W_t}{W_0} = \frac{D_t}{D_0} \tag{3.7}$$

$$D_0 W_0 L_0 = D_t W_t L_t \tag{3.8}$$

Using Eq.3.7;

$$Thickness = D_t = \left(\frac{W_t}{W_0}\right) D_0 \tag{3.9}$$

Using Eqs.3.7 and 3.8, true strain can be calculated as:

$$\frac{L_t}{L_{0-1}} = \left(\frac{W_0}{W_t}\right)^2 - 1 \tag{3.10}$$

Using Eq.3.7, true stress can be calculated from Eq.3.11

$$\frac{F_t}{(W_t D_t)} = \frac{F_t}{\left\{\left(\frac{W_t^2}{W_0}\right) D_0\right\}} \tag{3.11}$$

3.5.2 Instrumentation for Relaxation and Hysteresis Experiments

For the relaxation and some of the hysteresis experiments which were required for the theoretical calculations, a standard Instron 4411 tensile testing machine was used at Koc University.

3.5.3 Instrumentation for Differential Scanning Calorimetry

DSC analysis was performed using a TA Q1000 DSC in a dry nitrogen medium.

3.5.4 Instrumentation for Wide Angle X-Ray Scattering

Bruker AXS Generator equipped with a copper target tube and a 2-D detector were used to obtain the unique quadrant of the uniaxially oriented samples. The generator was operated at 40 kV and 40mA and beam was monochromatized at CuKα. Accumulation time of twenty minutes was used. The samples were placed 11.5 cm away from the detector.

3.6 Experimental Procedure

3.6.1 Experimental Procedure for the Automated Uniaxial Machine and WAXS

Two kinds of experiments were carried out on the automated uniaxial stretching machine: Uniaxial stretching and hysteresis. For both experiments, the cast films were cut into dumbbell shapes with narrowest width of 30 mm at 26 mm gauge length. The sample shape is designed so that it allows the use of transverse isotropy assumption safely.

For the uniaxial stretching experiment, the specimen is mounted on the clamps and stretched up to an engineering stretch ratio of five that is the upper limit of the machine for these specimen dimensions. In the hysteresis experiments, the specimen was first stretched up to a stretch ratio of 2 then unloaded and loaded again to a higher stretch ratio with stretch ratio increments of 0.5. The reloading process is applied until the maximum possible stretching limit of the machine is reached. In all experiments, the samples were stretched at a rate of 25 mm/min.

The samples were captured at the stretched state by rectangular picture frame sandwich clamps. WAXS data was taken at a series of times extending to a few days while the specimen was maintained in the stretched state. This process was employed in order to investigate the effects of stretching and long term holding on crystallization. The portion of the material within the clamps is chosen carefully such that it includes the central point where the width and birefringence measurements are made. This allows birefringence data to be compared with x-ray data and observe the effect of crystallization on the birefringence-true stress curve.

3.6.2 Experimental Procedure for Instron

Two kinds of experiments were carried on the standard Instron 4411 tensile test machine: Relaxation and hysteresis. The specimen was cut into dumbbell shapes with narrowest width of 4.76 mm at 24 mm gauge length which is in agreement with ASTM D 638M standard.

For the relaxation experiment, the specimen was mounted on the machine and stretched with a stretching rate of 500 mm/min up to a strain of 300%. Then the specimen was held at that position (constant strain) for thirty minutes and force vs. time data was collected.

For the hysteresis experiment, the specimen was mounted on the machine and stretched up to a stretch ratio of 2. Since the machine did not have a cyclic elongation mode, the experiment was stopped after first elongation, the direction of the experiment was changed and the specimen was retracted until zero force. This completed the first cycle. The other cycles were carried on similarly, but with increased stretch ratio with increments of 1 (such as stretch ratio = 3, 4, 5 etc.) for each cycle until the specimen failed. In all hysteresis experiments, stretching rate of 25 mm/min was used.

3.6.3 Experimental Procedure for Differential Scanning Calorimetry

Standard aluminum DSC pans are used with a sample weight ranging from 10 to 15 mg. The samples are placed in the DSC cell and cooled down to $-150°C$ using liquid nitrogen and heated up with a heating rate of 20°C/min to 250°C. The experiemtents were terminated at 250°C because thermal degradation can take place above this temperature. To get rid of the thermal history of polyurethanes, the samples are quenched down to $-150°C$ again by

using liquid nitrogen and heated up to 250°C.

Chapter 4

DERIVATION OF THE VISCOELASTIC WORK FUNCTION

4.1 Objective

When a viscoelastic material is deformed by the application of a cyclic force, some of the mechanical work required is stored in the material and the remainder is dissipated as heat. This energy dissipation or hysteresis in the material results from several different mechanisms which are dependent on the type of the material and the experimental conditions. The major sources of hysteresis can be listed as viscoelasticity, crystallization, breakdown of hydrogen bonds, changes in network configurations and changes in network structure. The energy lost may be dissipated as heat, consumed by morphological changes or go unmeasured during the time scale of the experiment. Consequently, part of the energy may be recoverable with time due to viscoelastic behavior of the TPUUs and part is permanently lost.

The objective of this chapter is to propose a model to calculate the amount of energy that is recoverable in hysteresis due to the viscoelastic nature of the TPUU's under consideration. The plastic portion which is permanently lost can then be calculated by subtracting the viscoelastic amount from total hysteresis.

4.2 Theory

In a uniaxial stress relaxation experiment, the sample is stretched up to a defined deformation. Keeping this deformation constant, the stress decay is recorded as a function of time. As schematically shown in Figure 4.1, the stress relaxes to a steady state value, which is nonzero for a solid.

To evaluate the relaxation curve, the applied stress σ is separated into two components, a relaxing stress component $\Delta\sigma$ and a time independent stress component σ_0:

$$\sigma(t) = \sigma_0 + \Delta\sigma(t) \tag{4.1}$$

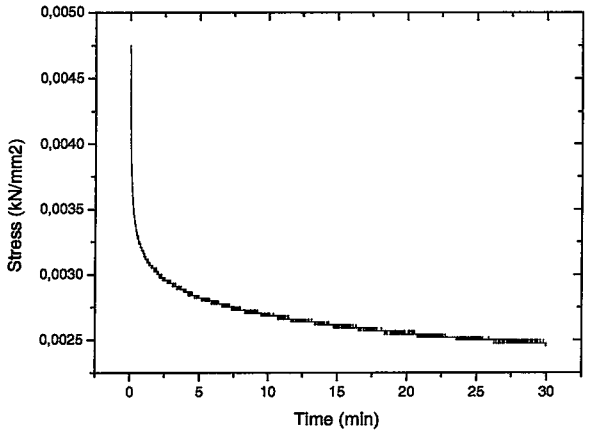

Figure 4.1: Stress relaxation experiment.

According to Seeger [49, 50], the relaxing stress component $\Delta\sigma(t)$ is called the thermal stress component, because it acts on short-range obstacles, which can be overcome by stress aided thermal activation. It also depends on the plastic deformation rate and the temperature. In contrast to the relaxing stress component, σ_0 is called athermal stress component. It is originated form long-range stress fields, which cannot be overcome by the thermal activation.

4.3 Derivation of the Work Function

In a stress relaxation experiment, one of the choices of a curve fit to experimental points is to make a power fit to the relaxing component and keep the non-relaxing component constant such as:

$$\sigma(t) = \sigma_0 + \Delta\sigma(t) = \sigma_0 + At^{-n} \tag{4.2}$$

where A is a constant, t is time and n is a number which is different for each material. Since n is specific to each material, it gives information about the time dependent behavior of that material. If the material behavior is linear, the stress can be represented by

$$\sigma(t) = E(t)\,\varepsilon \tag{4.3}$$

where the function E(t) is called relaxation modulus and ε is strain. From Eqns. 4.2 and 4.3;

$$\begin{aligned} \sigma(t) &= \sigma_0 + At^{-n} = E(t)\,\varepsilon \\ &\Rightarrow \quad E(t) = \frac{\sigma_0}{\varepsilon} + \frac{A}{\varepsilon}t^{-n} \end{aligned} \tag{4.4}$$

Eq. 4.4 can be further simplified as follows to find the form of E(t):

$$\frac{\sigma_0}{\varepsilon} = B;\ \frac{A}{\varepsilon} = C \Rightarrow E(t) = B + Ct^{-n} \tag{4.5}$$

The relaxation phenomenon is affected by the magnitude and sequence of stresses or strains in all of the past history of the material. Based on this fact, various mathematical methods have been suggested to represent the time dependence or viscoelastic behavior of materials in the literature.

Any stress-time curve may be approximated by the sum of a series of step functions which correspond to a series of step-like increments in load for a linear constitutive formulation. The relaxation modulus $E(t)$ may be defined as the relaxation stress resulting from unit of applied strain and is different for each material (a material property). By making use of the Boltzman superposition principle, the stress $\sigma(t)$ occurring during relaxation at time t may be represented as,

$$\sigma(t) = \int_0^t E(t-\tau)\frac{\partial \varepsilon}{\partial \tau}d\tau \tag{4.6}$$

where τ is any arbitrary time between 0 and t, representing past time.

The total time-dependent (viscoelastic) work per unit volume during one complete loading and unloading cycle can be calculated by integrating the increment of $\sigma d\varepsilon$ work done over a complete cycle of period T, as follows

$$\frac{\Delta W}{V_0} = \int_0^T \sigma \frac{d\varepsilon}{dt}dt \tag{4.7}$$

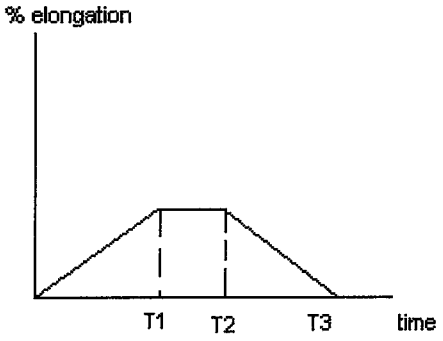

Figure 4.2: Loading and Unloading Pattern.

Just like stress, total viscoelastic work is affected by the magnitude and sequence of stresses or strains in all of the past history of the material. So again, by using Boltzman superposition principle and substituting the stress function from Eq. 4.6, viscoelastic work done per unit volume over a complete cycle of period T is:

$$\frac{\Delta W}{V_0} = \int_0^T \int_0^t \left(E\left(t-\tau\right) \frac{\partial \varepsilon}{\partial \tau} d\tau \right) \frac{\partial \varepsilon}{\partial t} dt \tag{4.8}$$

The loading and unloading pattern of the hysteresis experiments that were carried on Instron 4411 can be seen in Figure 4.2.

In Figure 4.2, loading begins when the time is zero and ends at T_1. The unloading takes place between time T_2 and T_3. As it can be seen, the hysteresis cycle is not continuous and there is a time delay (T_2-T_1) before unloading. This is due to the incapability of the tensile test machine which does not have a cyclic loading mode. After loading, each time one has to enter the software and change the direction of the experiment which results in time lost at constant strain. To be consistent, this time delay was kept constant (35 seconds for each sample) and the effect of holding the sample at constant strain between loading-unloading was taken into account during calculation of the work function.

Eq. 4.8 can be adapted to the loading-unloading cycle of the experiments which was plotted in Figure 4.2,

$$\frac{\Delta W}{V_0} = \int_0^{T_1}\int_0^{t}\left(E(t-\tau)\frac{\partial\varepsilon}{\partial\tau}d\tau\right)\frac{\partial\varepsilon}{\partial t}dt + \int_{T_2}^{T_3}\int_0^{T_1}\left(E(t-\tau)\frac{\partial\varepsilon}{\partial\tau}d\tau\right)\frac{\partial\varepsilon}{\partial t}dt + \int_{T_2}^{T_3}\int_{T_2}^{t}\left(E(t-\tau)\frac{\partial\varepsilon}{\partial\tau}d\tau\right)\frac{\partial\varepsilon}{\partial t}dt \tag{4.9}$$

To simplify,

$$\frac{\partial\varepsilon}{\partial t} = m;\ \frac{\partial\varepsilon}{\partial\tau} = m \tag{4.10}$$

$$\Rightarrow \frac{\Delta W}{V_0} = m^2\int_0^{T_1}\int_0^{t}\left[B + C(t-\tau)^{-n}\right]d\tau dt - m^2\int_{T_2}^{T_3}\int_0^{T_1}\left[B + C(t-\tau)^{-n}\right]d\tau dt + \int_{T_2}^{T_3}\int_{T_2}^{t}\left[B + C(t-\tau)^{-n}\right]d\tau dt$$

When the inner integrals are taken, 4.10 simplifies to:

$$\frac{\Delta W}{V_0} = m^2\int_0^{T_1}\left[Bt + C\left(0 - \frac{t^{-n+1}}{n-1}\right)\right]dt - m^2\int_{T_2}^{T_3}\left[BT_1 + C\left(\frac{(t-T_1)^{-n+1} - t^{-n+1}}{n-1}\right)\right]dt + m^2\int_{T_2}^{T_3}\left[B(t-T_2) + C\left(0 - \frac{(t-T_2)^{-n+1}}{n-1}\right)\right]dt \tag{4.11}$$

Taking the outer integral and making the corresponding simplifications, the final form of the viscoelatic work function becomes;

$$\frac{\Delta W}{V_0} = m^2B\left[\frac{(T_1)^2}{2} + \frac{(T_2)^2}{2} + \frac{(T_3)^2}{2} - T_1T_3 + T_1T_2 - T_2T_3\right] + \left[\frac{Cm^2}{n^2-3n+2}\right]\left\{(T_1)^{-n+2} + (T_2)^{-n+2} - (T_3)^{-n+2}\right\} + \left[\frac{Cm^2}{n^2-3n+2}\right]\left\{(T_3-T_1)^{-n+2} - (T_2-T_1)^{-n+2} + (T_3-T_2)^{-n+2}\right\} \tag{4.12}$$

4.4 Calculation of Relaxation Modulus

The required constants (such as B, C and n) to calculate the work function in Eq. 4.12 can be acquired from the relaxation curve. From Eq. 4.4;

$$\sigma(t) = \sigma_0 + At^{-n} = E(t)\,\varepsilon \tag{4.13}$$

If the non relaxing stress component σ_0 is taken to the left side and logarithm of both sides is taken;

$$\begin{aligned} \sigma(t) - \sigma_0 &= At^{-n} \\ \log(\sigma - \sigma_0) &= \log(A) - n\log(t) \end{aligned} \tag{4.14}$$

When $\log(\sigma - \sigma_0)$ is plotted versus $\log(t)$, a linear curve whose slope is n is acquired. The point where this curve intersects the y axis gives the logarithm of A. σ_0 is chosen from the stress-time curve and is equal to the value at which this curve settles for long times. Once A is calculated and σ_0 is chosen, B and C can be calculated from Eq. 4.5 as follows:

$$\frac{\sigma_0}{\varepsilon} = B; \frac{A}{\varepsilon} = C$$

Chapter 5

EXPERIMENTAL RESULTS

5.1 Results of the DSC Experiments

DSC analysis of polymers provides useful information about their temperature dependent transitions including the Tg which is the glass-rubber transition temperature and melting endotherm which is the crystalline-amorphous transition temperature. In previous work [51], it is detected with a great certainty that Tg is that of the soft segment in the polyurethane chains. The lower temperature endotherm is also attributed to the soft segment if the hard segment amount is low.

The solution cast polyurethanes are known to have a thermal history and heating them for the first time (first run) does not give enough information on the thermal behavior of hard and soft segments [13, 32]. In order to get rid of this, the material is brought to $-150°C$ by quenching after the first run. The second heating curve gives the thermal characteristics of the polymer more accurately. The effect of hard segments at high temperatures cannot be observed in this run since its percentage is not more than 30% in all materials used in this thesis.

Table 5.1: Thermal properties of some of the samples

Material	Tg ($°C$)	Tc ($°C$)	Tm ($°C$)
PT-ED-20	-77	-23	20
PE-HMDA-20	-54	-5	34
PE-ED-20	-58	-12	30

Important features of the samples during the second heating are reported in Table 5.1. For PT-ED-20, a Tg of $-77°C$ was observed which is close to Tg of PTMO (soft segment). The small difference in Tg's of the polymer and PTMO arise from the fact that although the hard segment content is low in this material, there is still an interaction between the soft

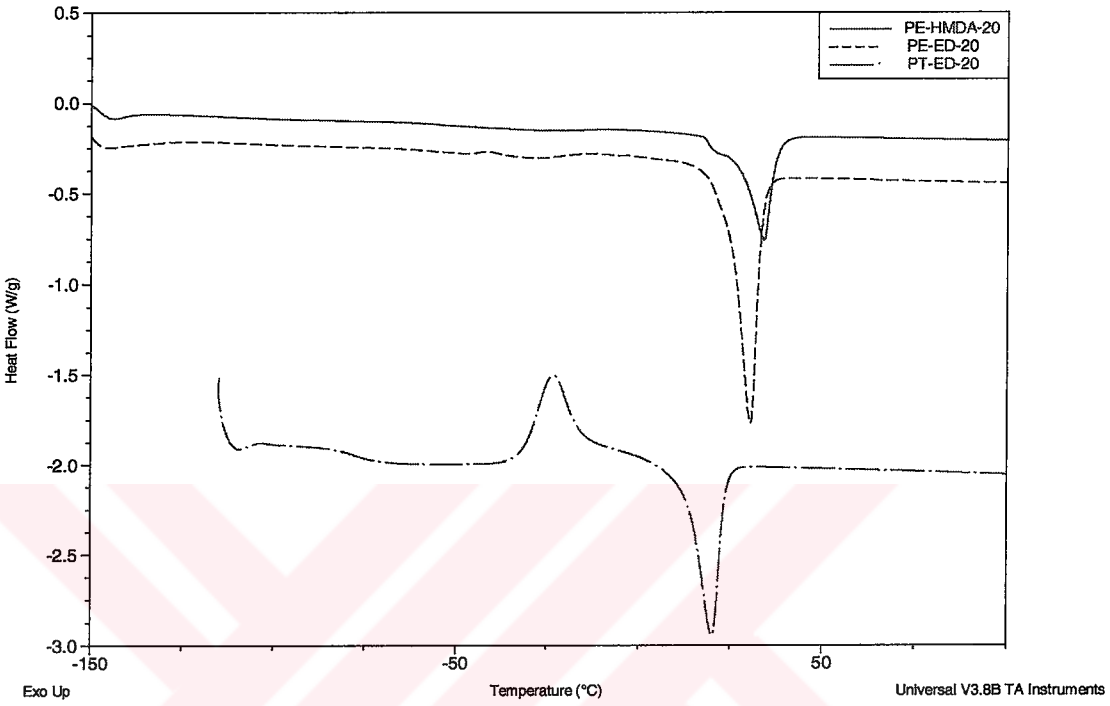

Figure 5.1: DSC results.

and hard segments. A melting endotherm is observed at around $20°C$ in PT-ED-20 which is characteristic of a crystalline PTMO phase. Hu et al. [52] presented a rationalization for the degree of phase separation in segmented polyurethaneureas that is related to crystallizability of the soft segment. Hu et al. [52] and Cooper and Wang [13] showed that the presence of a PTMO melting endotherm in the PTMO-2000 series correlates with improved microphase separation. In PE-HMDA-20 and PE-ED-20 samples, a Tg of $-54°C$ (PE-HMDA-20) to $-58°C$ (PE-ED-20) is observed, indicating that HMDA has a more pronounced effect on the Tg of the soft segment, PEO.

While the crystallization peak of PT-ED-20 can be clearly seen from Figure 5.1, there is a relatively very small crystallization peak for the two PE based samples. Since the only difference between PT-ED-20 and PE based samples is the soft segment, this can be attributed to different crystallization behavior of the soft segments. While the small

crystallization peak of PE samples is an indication of PE's more flexible structure, the evident crystallization peak of PT-ED-20 shows that PTMO is more easily crystallizable. Also while the range of glass transition temperature is narrow for PT-ED-20 (about $40°C$), it is wider for PE based samples (about $100°C$). This suggests a higher degree of structural heterogeneity in the PE based samples in which small bundles of hard segments are more or less solubilized in the soft segment phase.

The melting endotherms for the two PE samples are different. The PE-HMDA-20 curve, which contains HMDA as the chain extender, is shifted to the right and the endotherm area under the PE-ED-20 curve, which contains ED as the chain extender, is larger. This indicated that more crystallization is observed in PE-ED-20 than PE-HMDA-20 which can solely be attributed to the chain extender.

The range of melting temperatures is larger for PT-ED-20 than PE-ED-20 indicating that there is stronger interaction and mixing of segments in the former.

5.2 Results of Uniaxial Stretching and WAXS Experiments

The tensile behavior of thermoplastic elastomers generally depends on (i) the size, shape, and concentration of the hard domains [53, 54], (ii) intermolecular bonding within the hard domains, (iii) the ability of the soft segment to crystallize under strain [13], and (iv) the extent of microphase separation. A high level of microphase separation in amine extended systems has been attributed to a larger number of possible hydrogen bonds between hard segment chemical bonds [26].

5.2.1 Effect of Soft Segment

Figure 5.2 shows the room temperature true stress-true strain-birefringence behavior of the materials whose hard segment concentration is 30% (by weight). The curves are obtained from samples stretched to a stretch ratio of 5 which is smaller than the failure stretch ratios. To show the effect of soft segment, results for two samples with different soft segments but the same chain extender are compared on the same graph. WAXS data, shown in the figure, are taken at the state indicated by the arrows. The WAXS readings were taken offline while the specimen was being held in the stretched state by the clamps as explained above. The corresponding birefringence-true stress curves are given as insets in Figure 5.2.

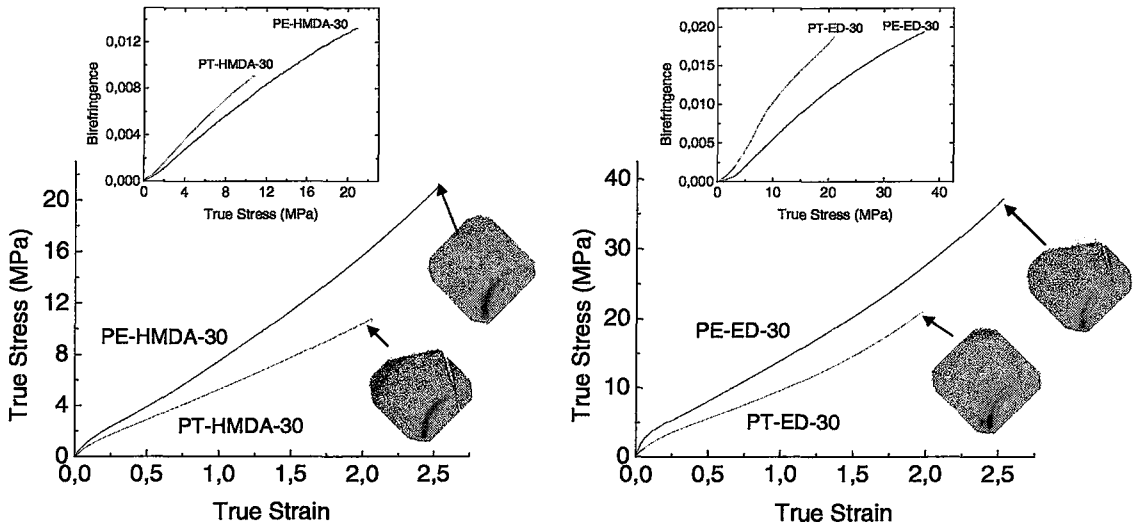

Figure 5.2: Effect of soft segment on True Stress vs True Strain for HS=30%.

As can be seen from Figure 5.2, the samples whose soft segment is PEO show larger true stress values than the ones with PTMO no matter which chain extender is used. This is probably due to the urea groups that the amine terminated PEO based TPUUs contain. On the other hand, since PTMO is hydroxy terminated, it forms urethane groups during the prepolymer stage. Urea groups are generated during chain extension. Since urea groups form much stronger intermolecular hydrogen bonding than urethanes [53], PEO based polymers show larger true stress values than their PTMO based analogues. This observation is also supported by consideration of the differences in the Tg values of $-77°C$ for PTMO and $-55°C$ for PEO. At room temperature, PEO is closer to its glass temperature and is therefore stiffer than PTMO.

When the crystallization patterns are investigated, it is seen that the unstretched sample whose soft segment is PTMO has an amorphous halo since the melting point of PTMO crystal (10°C) is below room temperature at which the experiments are performed. After stretching, PTMO samples show crystallization upon deformation as indicated by the corresponding WAXS patterns in Figure 5.2. PTMO is known to be easily crystallizable which explains this behavior. In a previous work, it was concluded by Yeh et al., [55] that the two peaks that can be observed starting from 200% strain are indicative of strain-induced

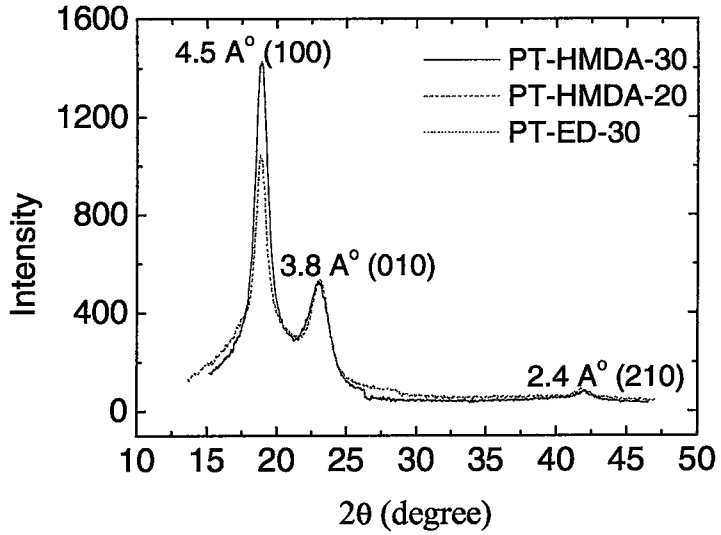

Figure 5.3: WAXS equatorial intensity profile for some PT samples stretched to a stretch ratio of 5.

crystallization of the PTMO. According to the same study, with the increase of strain (up to 700%), the crystalline regions become stronger and more oriented, whereas the unoriented amorphous phase becomes weaker. The equatorial intensity profiles from WAXS patterns at 500% strain are presented in Figure 5.3. It appears that PTMO based samples show strain induced crystallization with essentially needle like crystals in which the polymer chains exhibit nearly perfect chain orientation with deformation. The WAXS pattern shown in Figure 5.3 indicates that the azimuthal distribution of equatorial crystalline peak is extremely narrow. This peak would not exist unless the polymer chains lose their entropy to create near perfect alignment. These results are in agreement with the conclusions of Bonart [4].

On the other hand, samples with PEO soft segments show little or no crystallization according to WAXS patterns taken right after the stretching, as can be seen from the x-ray patterns presented in Figure 5.2. This difference between the crystallization behavior of the two soft segments can be explained as follows: The PT segment may be modeled as a chain of freely jointed rods where the butyl groups act as rods and the oxygen in between acts as the freely rotating joint. The PE segments are also similar, but the ethyl group

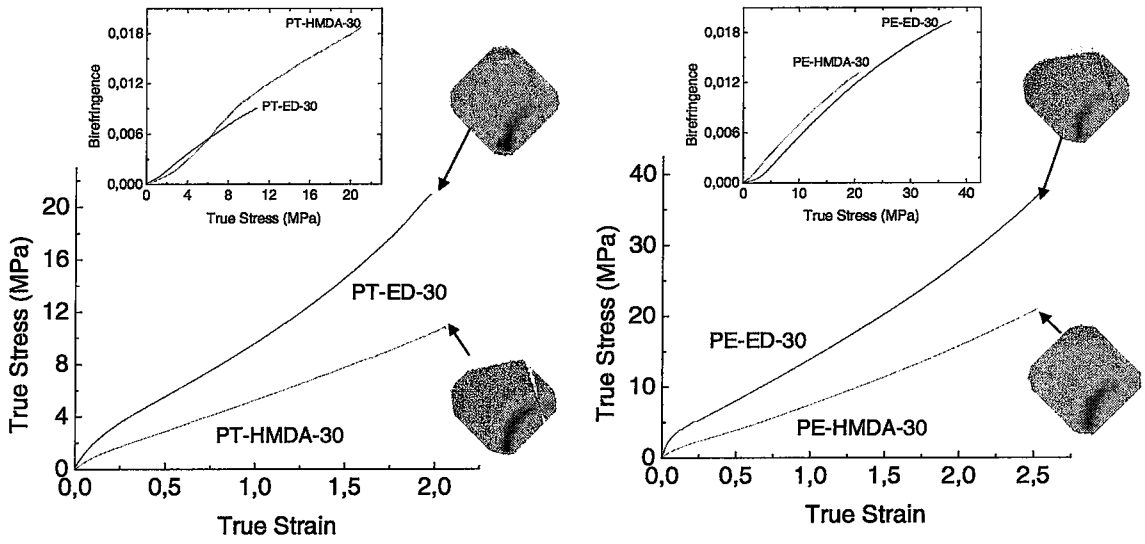

Figure 5.4: Effect of hard segment on True Stress vs True Strain for HS = 30%.

constituting the stiff part is much shorter than the butyl group of PT. It is well known that in chains of rigid rods separated by flexible joints, crystallization takes place readily when the rod-like parts are longer [56]. Therefore, crystallization in PT samples is much more readily expected. The birefringence vs. true stress curves of PT samples fall above the corresponding curves for the PEO segments.

5.2.2 Large Deformation Stress Optical Behavior

Collectively the stress optical behavior of these materials can be categorized as "three-regime" behavior. Regime I, covering the lowest stress-range, is the smallest of the three regimes. Following this regime, there is a rapid upturn into Regime II that leads to Regime III that has intermediate slope as the polymers presumably reaching their finite extensibilites. Inasmuch as birefringence is a measure of segmental orientation, these results indicate that the PTMO groups orient more than the PEO groups at corresponding strains.

5.2.3 Effect of Hard Segment

Figure 5.4 shows the room temperature true stress-true strain behavior of the materials whose hard segment concentration (HS) is 30%. The data is presented such that the samples that are based on the same soft segment are plotted on the same graph to show the effect of chain extender. The corresponding birefringence-true stress curves are given as insets in Figure 5.4. The samples with chain extender ED show larger true stress values than the ones with HMDA, because each repeat unit of ED contains 2 CH_2 groups while that of HMDA contains 6 CH_2 groups, and the shorter chains are known to contribute more to stress at the same extension ratio. Irrespective of the soft segment type, the ED chain-extended ones exhibit higher crystallinity than the HMDA ones as can be seen from WAXS patterns in Figure 5.4. Wilkes et al. [8] observed two different types of order within the hard segment domains corresponding to two different chain extenders and attributed these to differences in the extent of molecular fit within the hard segments. This feature relates to entropy differences between the two types of chain extenders, ED $(CH_2)_2$ and HMDA $(CH_2)_6$. Assuming that each C-C bond can be in one of three possible rotational states, the number of different configurations which the two chain extenders can take may be estimated [57, 58]. Since, ED has a single rotatable bond it can be in three different states in the network, whereas HMDA with five rotatable bonds can take up to 35 different configurations. This leads to larger entropy changes upon deformation of HMDA extended ones than ED. As a result of this difference, samples with the ED have little entropy to lose upon stretching and readily crystallize, whereas the ones containing HMDA has a large amount of entropy to lose and is therefore more difficult to crystallize. It is also worth noting that HMDA acts like a more flexible hinge for the two rigid segments flanking it on its both sides. Alternatively, ED acts like a stiffer hinge for its flanking rigid neighbors.

5.2.4 Effect of Hard Segment Concentration

Although the samples with hard segment content of 30% have been used to explain the effect of soft and hard segments in the discussion above, a comparison with the ones with HS=20% can be helpful in explaining the contribution of hard segment concentration to mechanical behavior.

Figure 5.5 gives the true stress-true strain-birefringence data for PT-HMDA samples

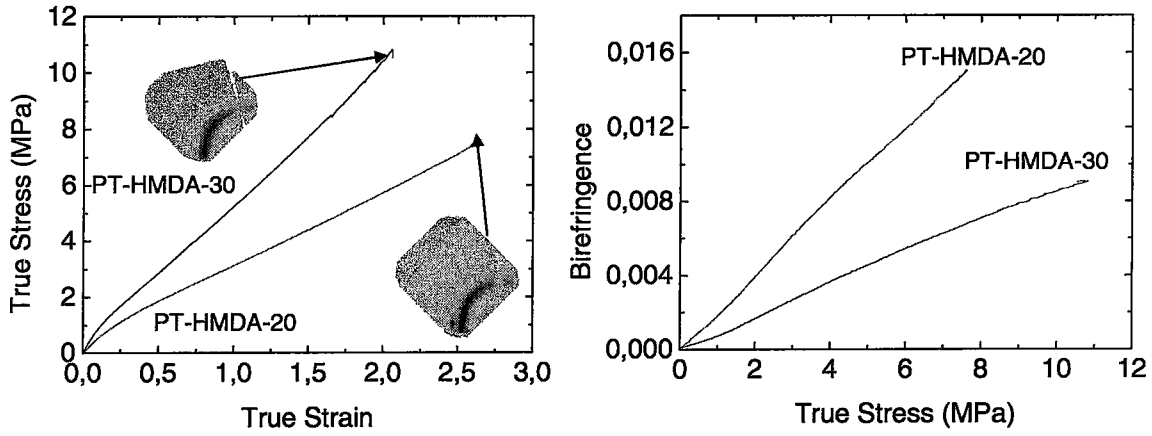

Figure 5.5: True sress-true strain-birefringence values for PT-HMDA with HS = 20% and HS = 30%.

whose hard segment percentages is either 20% or 30%. The left panel shows the stress-strain results, and the right panel shows the birefringence results. As can be seen from this figure, the PT sample with higher hard segment concentration shows larger true stress values. This is expected since the hard segment is the part which gives high strength characteristics to TPUU's. When compared from crystallization point of view, a better orientation scheme is observed in the low hard segment content sample. Upon decreasing the hard segment content, a transition of morphology from interconnecting hard and soft segment domains to isolated hard segment domains in a soft segment matrix was observed by Cooper et al. [13] This may explain the better phase separation and crystal structure in PT samples with the low hard segment content.

Figure 5.6 shows the true stress-strain values for PT-ED samples with HS=20% and HS=30%. Again the sample with higher hard segment concentration shows larger true stress values. The third peak that is observed at about $2\theta = 42.5°$ in Figure 5.3, is slightly observable in the upper left portion of the WAXS pattern of 30% sample but cannot be seen for 20%. This peak was attributed to strain induced crystallization of PT [55]. So it can be said that strain induced crystallization of PT is more pronounced as hard segment content increases.

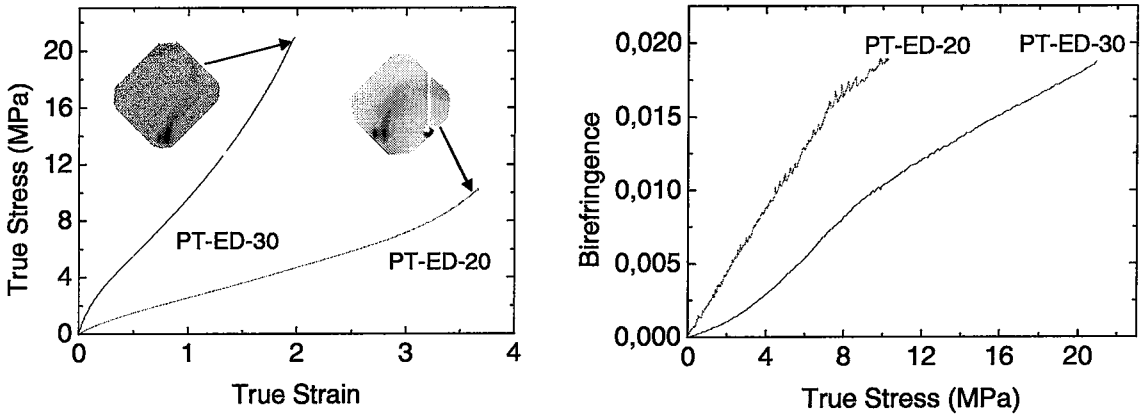

Figure 5.6: True stress-true strain-birefringence values for PT-ED with HS = 20% and HS = 30%.

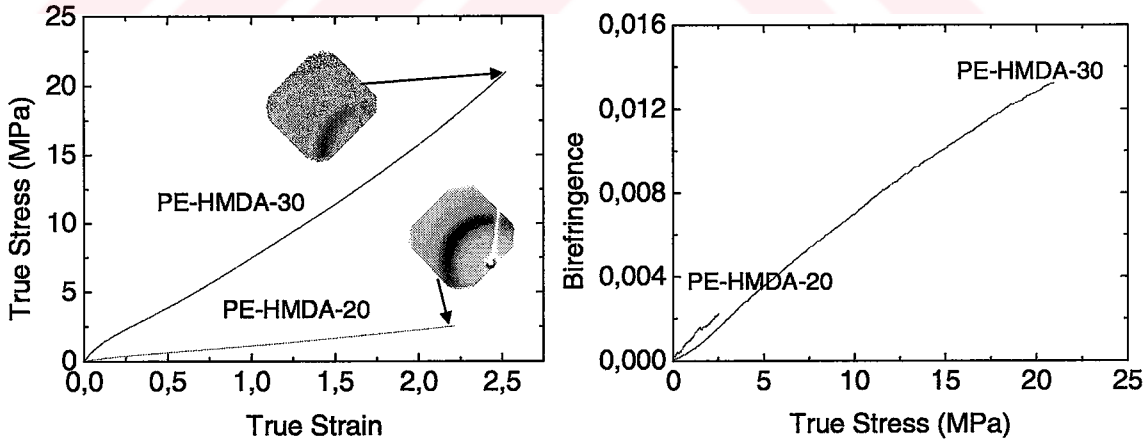

Figure 5.7: True stess-true strain-birefringence values for PE-HMDA with HS = 20% and HS = 30%.

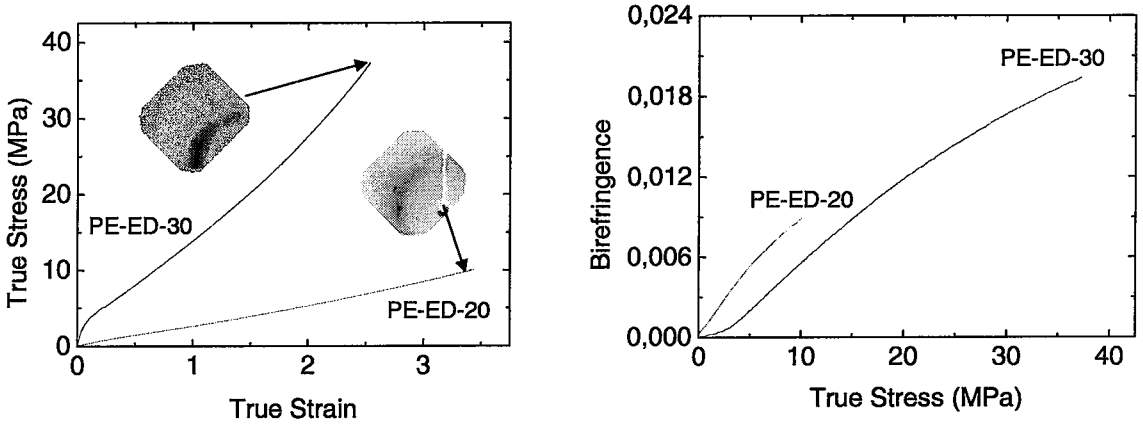

Figure 5.8: True stress-true strain-birefringence values PE-ED with HS = 20% and HS = 30%.

In Figure 5.7, true stress-true strain-birefringence data for PE-HMDA-20 and PE-HMDA-30 are given. The same behavior, namely, larger stress values for high hard segment concentration can be observed for PE-HMDA. However, there is no crystallization for both PE-HMDA samples, which may clearly be attributed to the role of the PE groups, as discussed above.

True stress-true strain-birefringence graphs for PE-ED samples with different hard segment contents (either HS=20% or HS=30%) are plotted in Figure 5.8. There is a remarkable effect of hard segment concentration on the stress-optical behavior. The Regime I is present in the PE-ED-30 is suppressed in PE-ED-20 where only the linear stress optical rule followed by saturation at high stresses is observed. Both samples undergo crystallization and exhibit near perfect chain orientation along the stretching direction as may be seen from the WAXS data. While PE-ED-20 containing smaller fraction of hard segments forms a well organized three dimensional lattice structure (presence of off equatorial peaks and their sharpness indicates this), increasing hard segment content appear to suppress this organization as the crystalline peaks are slightly broader. This is most likely due to steric hindrance effect on crystallizing species in the presence of larger fraction of rigid hard segments.

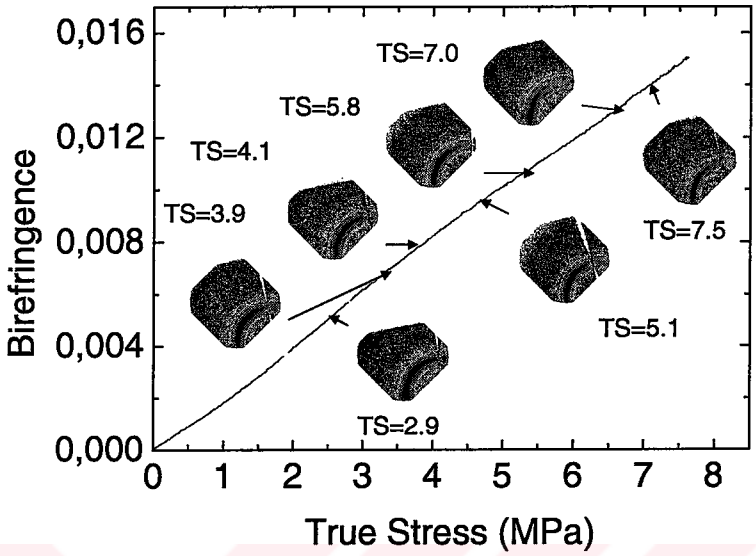

Figure 5.9: WAXS data taken at different True Stress values for PT-HMDA-20.

5.2.5 WAXS at Different True Stress Values for PT-HMDA-20 and PT-HMDA-30

X-ray data at different stretch ratios of PT-HMDA for HS=20% and HS=30% can be seen in Figure 5.9 and Figure 5.10 respectively. The true stress values at which the WAXS readings are made are indicated by TS in the figures.

When Figure 5.9 is compared with Figure 5.10, it is quite interesting to observe that the crystallization sets in at very high true strain values for the low hard segment concentration sample but spreads out more on the PT-HMDA-30. The crystallization is accompanied by a slight upturn on birefringence-true stress curve in PT-HMDA-20. It is important to note that the at least three stress optical regimes are discernible in both Figure 5.9 and Figure 5.10. Initial linear regime gives way to Regime II with steeper slope near 1-2 MPa. This slightly longer regime straightens out at higher stress levels. Remarkably, we do not see any evidence of expected leveling off in these curves. In fact we note a slight further positive deviation accompanying the appearance of equatorial diffraction peaks. In the absence of off equatorial peaks this peak can be categorized as "nematic-like" as it exhibits above

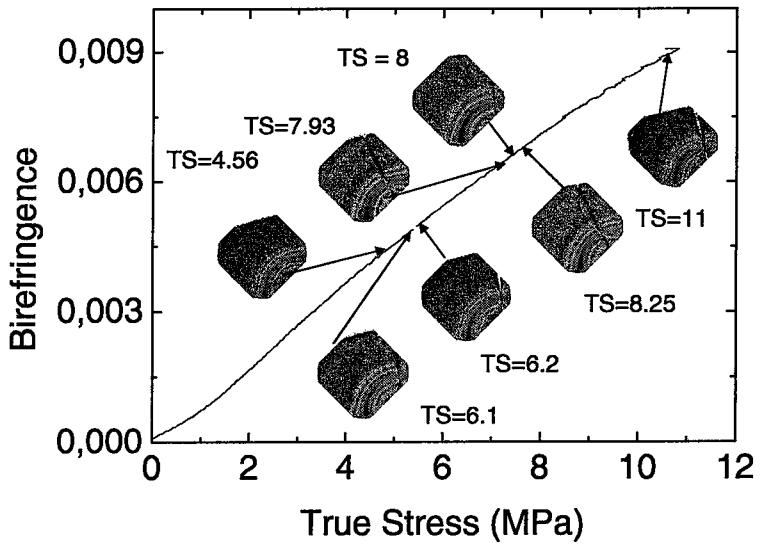

Figure 5.10: WAXS data taken at different True Stress values for PT-HMDA-30.

mentioned near perfect orientation. Evolution of crystalline peak is more gradual in PT-HMDA-30. But the developed equatorial peak is broader indicating lateral packing order of these "nematic-like" regions is poorer presumably reflecting the steric hindrance effects of the increased population of hard segments.

5.2.6 Effect of Strain Rate for PT-HMDA-20 and PT-HMDA-30

The true stress-true strain curves of the same materials (PT-HMDA-20 on the left and PT-HMDA-30 on the right) at different strain rates and corresponding WAXS patterns are presented in Figure 5.11. The rates, 2 mm/min, 25 mm/min, 200 mm/min are indicated in the figure. For both materials, the largest stress values are observed for the fastest strain rate. The low hard segment content PT sample shows better crystallization when stretched at the slowest rate, 2 mm/min. Crystallization decreases with increasing strain rate as can be seen from the respective WAXS data in Figure 5.11. On the other hand, the crystallization of high hard segment content PT is the opposite and crystallization increases with increasing strain rate.

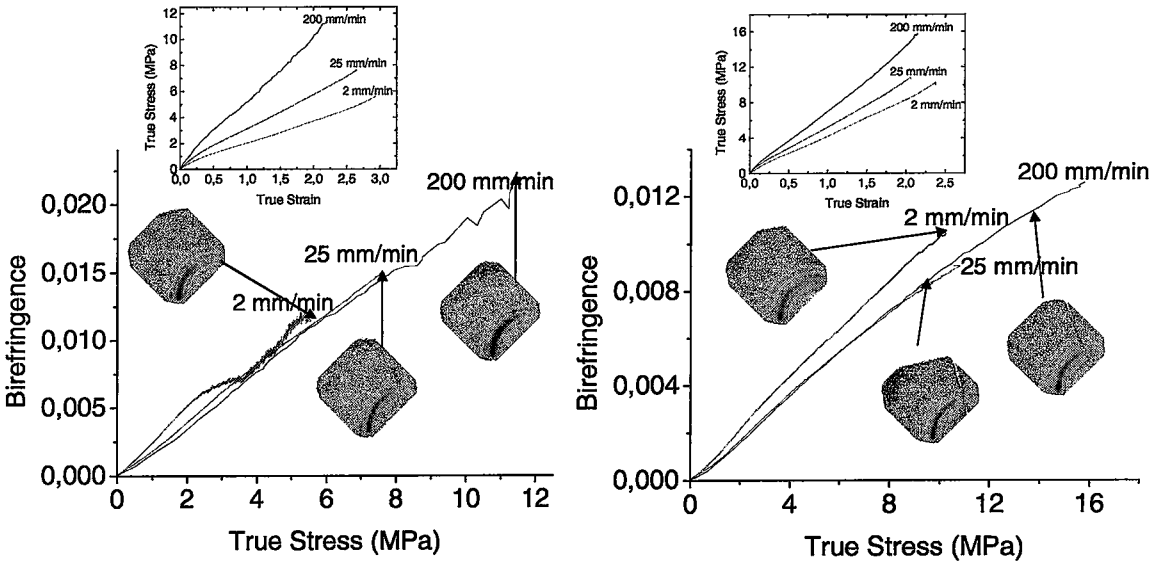

Figure 5.11: Effect of strain rate on Birefringence-True Stress curves of PT-HMDA-20 and PT-HMDA-30.

There is considerable detail in the WAXS patterns of PT-HMDA-20 and PT-HMDA-30 as they are affected by the stretching rate. The PT-HMDA-20 samples containing smaller fraction of hard segments exhibit lower orientation (compare the azimuthal spread of the equatorial nematic-line diffraction peak) as compared to those of PT-HMDA-30. In addition the faster the stretching rate is employed the narrower this peak becomes in PT-HMDA-20. This suggests that at slower deformation rates more of the crystallizable segments –however disorganized they are- gets into registry with one another and contribute to this peak if they are sufficiently oriented parallel to one another. Increasing stretching rate (suppression of relaxation mechanism) eliminate the formation of the latter disordered regions that are responsible for broadening the equatorial peak at low rates. Clearly PT-HMDA-30 data indicate that the crystallizable segments need to be more oriented to register with one another (lower azimuthal spread) to contribute to the broader equatorial peak otherwise they would not exist at all. Faster stretching certainly promotes this mechanism in the presence of higher fraction of harder segments.

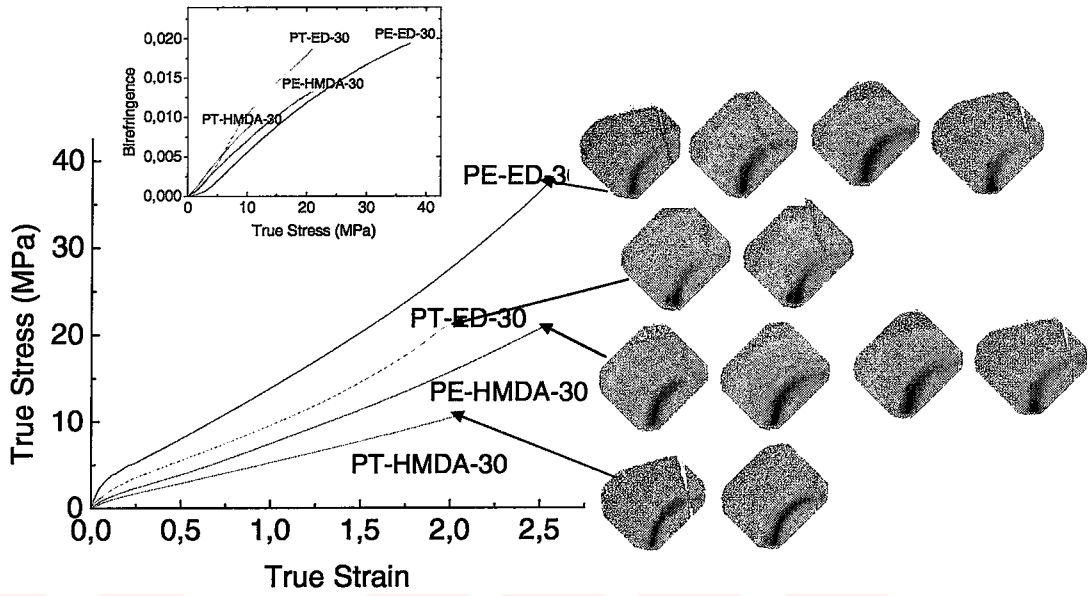

Figure 5.12: True Stress vs True Strain for all samples with HS=30%.

5.2.7 General Behavior for Samples of HS = 30%

In Figure 5.12, we compare the true stress-true strain and birefringence-true stress behavior of all HS=30% samples. The measurements are coupled with repeated offline WAXS data taken at the strains indicated by the arrows. The first WAXS is taken right after the stretching and the rest is taken in the following days (one day between each experiment) while the specimen is still kept at the stretched position within the clamp. The effects of soft and hard segments of the same samples were explained previously. All materials display the typical behavior of elastomers; with stress-strain behavior primarily depending on composition. It was also observed from the experiments that have been carried on a standard Instron machine that PE series extend to much higher stretch ratios than PT. Since elongation is usually related to soft segments, this can be attributed to the characteristic behavior of PEO that gives the material more flexibility than PTMO. The interesting point in the WAXS patterns is the crystallization behavior of the PE samples. As explained above, PE samples show little (PE-ED-30) or no crystallization (PE-HMDA-30) at the end of stretching. But while the sample is kept at the stretched position within the clamp,

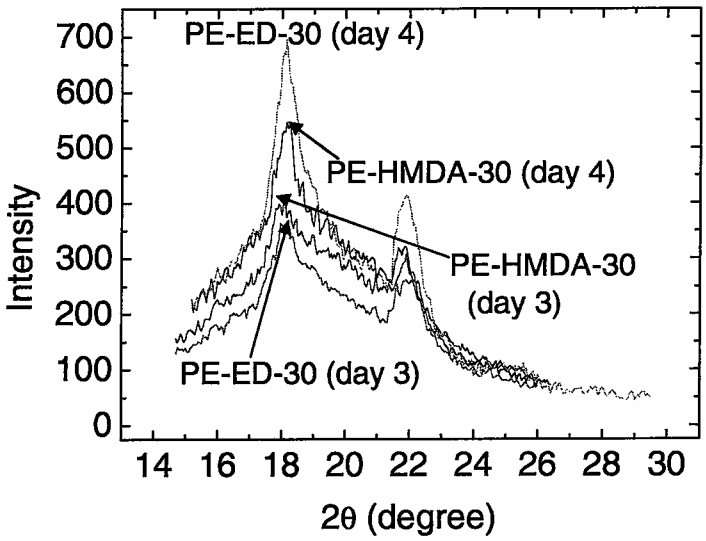

Figure 5.13: WAXS equatorial intensity profile for some PE samples stretched to a stretch ratio of 5.

the PE-ED-30 sample gradually developed highly oriented crystalline peaks superposed to amorphous halo over time. During this holding stage, the relaxation gradually brings the chains that were highly oriented but unregistered to laterally and axially registered state for them to form three dimensionally ordered crystalline state. This is quite pronounced in PE-ED-30 and PE-HMDA-30.

Figure 5.12 also shows the birefringence vs true stress values for the samples with HS = 30%. The stress optical law relates the birefringence and stresses applied in a system. The law follows a linear behavior of the birefringence with the stress as shown by the equation $\Delta n = C * \sigma$ where Δn is the birefringence, C is the stress optical constant, and σ is the true stress. An increase in birefringence is observed beginning from the start of stretching. Real time birefringence system data allows us to observe a very small linear portion on the true stress vs. birefringence curves, which obeys the stress optical law. The reason for this is because these materials should not be considered similar to standard amorphous materials. The main reason is because the hard segments are forming the long range physical network and since they exist at very early stages, then they rapidly make this relationship

non-linear. According to past experience, prior to crystallization linearity of birefringence stress is preserved. But if crystallization is induced, non-linearity is acquired immediately due to long range connectivity through the connected formed crystallites together with entanglements and hydrogen bonds. The stress optical coefficients for all samples may be determined from the linear portion of the birefringence vs. true stress curves (Figure 5.12) and by the use of stress-optical law. The results are presented in Table 5.2.

Table 5.2: Stress optical constants C, in GPa^{-1} from stretching data

PT-HMDA-20	1.8	PT-HMDA-30	0.3
PT-ED-20	2.2	PT-ED-30	0.4
PE-HMDA-20	1.0	PE-HMDA-30	0.4
PE-ED-20	0.9	PE-ED-30	0.1

5.2.8 Results of Hysteresis and WAXS Experiments

The mechanical hysteresis of a polymer represents the fractional energy lost as a result of subjecting that material to a defined deformation cycle. As with other elastomers, it can occur in polyurethanes due to a number of mechanisms such as (i) internal friction as segments of polymer molecules slide past each other as the molecules change their conformations during the deformation cycle, and (ii) strain induced crystallization as aligned segments crystallize during loading and plastic deformation of the second phase domains [29].

The true stress-strain hysteresis curves for the materials stretched to 2x, 2.5x, 3x, 3.5x and 4x at room temperature and subsequently retracted to zero force are presented in Figure 5.14. WAXS data is taken at the end of 4x while the specimen was being held within the clamps as explained earlier. First WAXS pattern was taken right after the stretching and the second one was taken one day later while the specimens were held stretched within the frames. The corresponding birefringence graphs are plotted in Figure 5.15.

For all the samples, the hysteresis loop (thus the energy lost) increases as the stretch ratio in cyclic loading increases. The greatest increase is observed for PT-ED (most crystalline sample) and the smallest for PE-HMDA (least crystalline sample). This is due to different

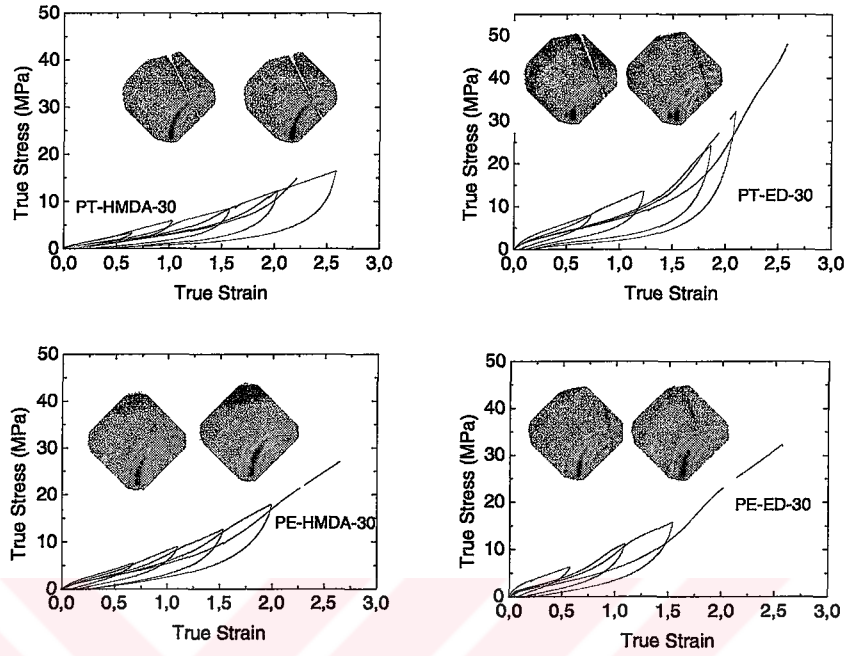

Figure 5.14: Hysteresis True Stress-True Strain Values for all samples with HS=30%.

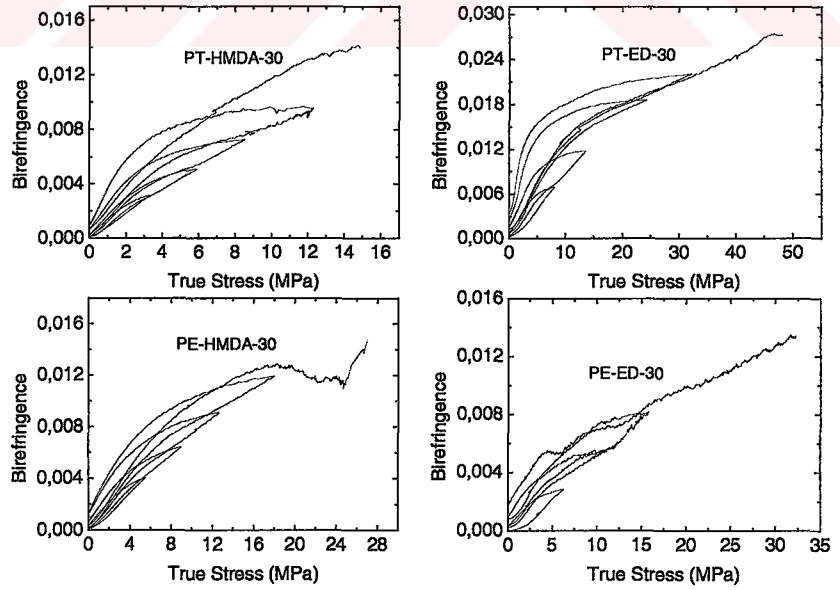

Figure 5.15: Hysteresis Birefringence Values for all samples with HS =30%.

mechanisms of deformation operating during stretching and retracting. During stretching, the molecules are re-organized; aligning themselves along the stretching direction. If the deformation is high enough, some of the chemical bonds, specifically the hydrogen bonds, can break; leading to disentanglement in the network. Rupturing of the hydrogen bonds leads to molecular slippage, chain disentanglement, phase mixing, soft segment crystallization, and the reformation of new bonds in the stretch configuration [28]. As deformation increases, crystalline regions begin to form; making the network more complex. On retraction from high deformations, the network cannot recover totally. This leads to an energy difference that can be observed as a loop at the stress-strain curve. This kind of energy loss is less pronounced for lower stretch ratios where permanent deformation hardly takes place.

The only difference between the crystallization patterns of the samples subject to hysteresis and the ones that were stretched uniformly is that the crystals are more clearly observable under hysteresis showing that cyclic loading-unloading of the samples finally results in better orientation of the polymer network than simply stretching. The unique crystallization behavior of PE samples (crystallization under relaxation) is again observed in hysteresis. There is also considerable hysteresis and a very small linear region in birefringence graphs.

Chapter 6

THEORETICAL RESULTS

6.1 Calculation of Viscoelastic Work Function for PT-ED-20

The theory behind the viscoelastic work function and the derivation were described in Chapter 4. In this chapter, the theory is coupled with the relaxation and hysteresis experiments that were carried on Instron 4411. The experimental procedure for relaxation and hysteresis were explained in detail in Chapter 3. Here calculation of the viscoelastic work function for PT-ED-20 is given as an example to show the procedure. The work values for other cycles and other materials were calculated similarly.

The stress relaxation curve of a PT-ED-20 sample that was stretched up to a strain of 300% with a strain rate of 500 mm/min and that was held at constant strain for 30 minutes can be seen in Figure 6.1. The reason for using 300% strain for the relaxation experiments is that different strains were tried and 300% was the most suitable one for power fit.

As it can be seen from Figure 6.1, the non relaxing component for this curve is about 0.0025 kN/mm^2. This number is subtracted from all stress values and the logarithm of both sides are taken. Then log (σ-σ_0) is plotted versus log (time) which can be seen in Figure 6.2.

A linear plot whose slope is n is expected when log (σ-σ_0) is plotted versus log (time). But as it can be seen from Figure 6.2, this curve is not linear for all time ranges, but for shorter times. To analyze the time effect on the material and calculate the required constants, it is better to consider the short times which give a linear region. In this study, this time is chosen to be 100 seconds and the resulting curve for PT-ED-20 can be seen in Figure 6.3.

The constant n is obtained from the slope of the curve in Figure 6.3 as 0.25. From the intersection point, A is found to be 0.00215. B and C are calculated as:

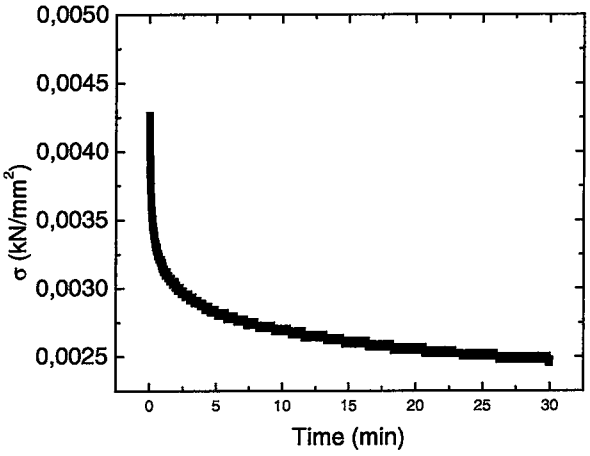

Figure 6.1: Stress relaxation curve of PT-ED-20.

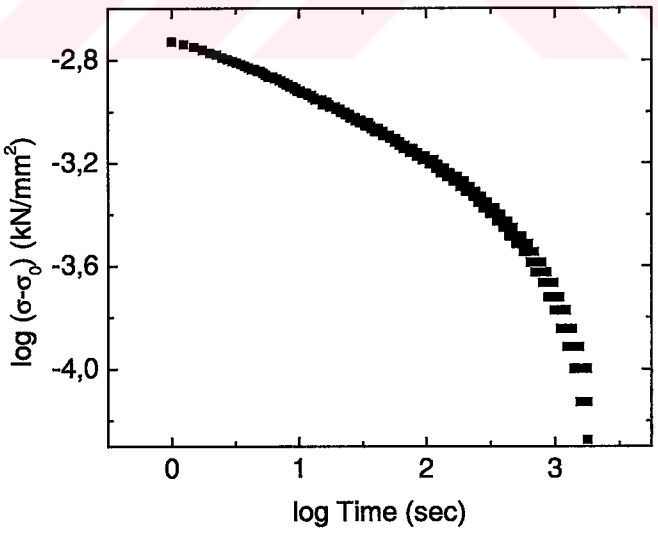

Figure 6.2: Log (σ-σ_0) vs. Log (t) for PT-ED-20 for 30 minutes

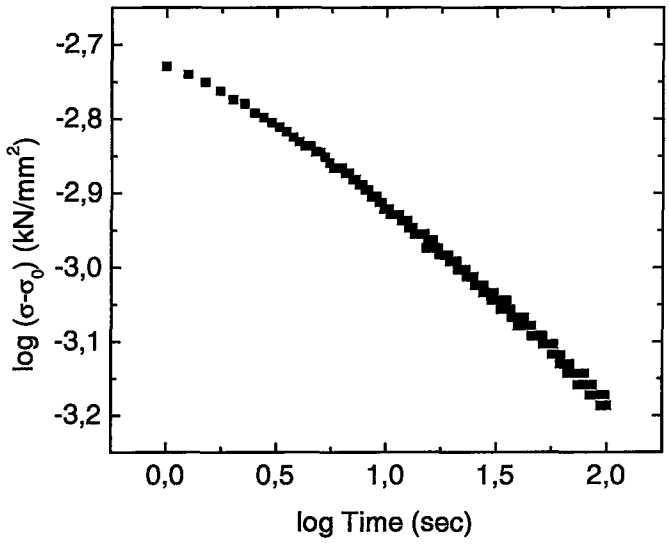

Figure 6.3: Log (σ-σ_0) vs. Log (t) for PT-ED-20 for 100 seconds

$$\frac{\sigma_0}{\varepsilon} = B \Rightarrow B = \frac{0.0025}{3} = 8.3 \times 10^{-4}$$
$$\frac{A}{\varepsilon} = C \Rightarrow C = \frac{0.00215}{3} = 7.1 \times 10^{-4}$$

The derived viscoelastic work function was:

$$\begin{aligned}\frac{\Delta W}{V_0} &= m^2 B \left[\frac{(T_1)^2}{2} + \frac{(T_2)^2}{2} + \frac{(T_3)^2}{2} - T_1T_3 + T_1T_2 - T_2T_3\right] \\ &+ \left[\frac{Cm^2}{n^2 - 3n + 2}\right]\left\{(T_1)^{-n+2} + (T_2)^{-n+2} - (T_3)^{-n+2}\right\} \\ &+ \left[\frac{Cm^2}{n^2 - 3n + 2}\right]\left\{(T_3 - T_1)^{-n+2} - (T_2 - T_1)^{-n+2} + (T_3 - T_2)^{-n+2}\right\}\end{aligned}$$

According to the formula, loading and unloading times such as T_1, T_2 and T_3 of the experiment are required. Since the initial gauge length is 24 mm, the time required to elongate the material to an elongation of 100% (24 mm) is equal to 57.6 seconds with a strain rate of 25 mm/min. So T_1 in the viscoelastic work function is equal to 57.6 seconds.

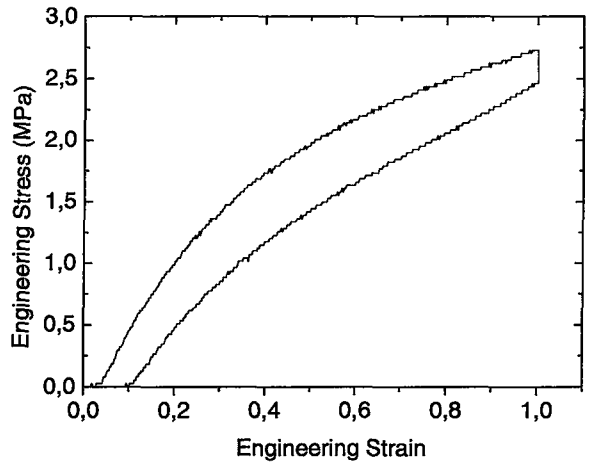

Figure 6.4: Hysteresis curve for the first cycle of PT-ED-20

As it was explained, the machine does not have a cyclic loading mode so there is a time delay of 35 seconds between loading and unloading which makes T_2 equal to 92.6 seconds. The unloading also takes 57.6 seconds since it is performed with the same speed (25 mm/min) that makes T_3 equal to 150.2 seconds. When all the constants are substituted in the viscoelastic work function, the result is calculated as 0.009 Nm. This is the amount of work that is recoverable with time for one cycle in which the sample is elongated to a maximum stretch ratio of 2 (elongation 100%).

The experimental hysteresis curve for the first cycle of PT-ED-20 can be seen in Figure 6.4. The amount of total hysteresis is acquired by calculating the area between the loading-unloading curves. For PT-ED-20, this value is equal to 0.022 Nm. This value constitutes of the viscoelastic hysteresis that is recoverable and the plastic hysteresis that is permanently lost. The viscoelastic hysteresis that is recoverable is calculated as 0.009 Nm. So plastic hysteresis is equal to 0.013 which is obtained by subtracting 0.009 Nm from 0.022 Nm.

6.2 Calculation of Viscoelastic Work Function for Four Samples

Table 6.1 gives the calculated results for a hysteresis cycle in which the maximum stretch ratio is 2 (elongation 100%) for four materials. The first column gives the nomenclature

Table 6.1: Results for a cycle in which the maximum stretch ratio is two

Material	W_T(Nm)	H_T(Nm)	H_{VE}(Nm)	H_P(Nm)
PT-ED-30	0.145	0.042	0.015	0.027
PT-ED-20	0.084	0.022	0.009	0.013
PE-HMDA-30	0.16	0.075	0.022	0.053
PE-HMDA-20	0.038	0.021	0.013	0.008

Table 6.2: Percentage results for a cycle in which the maximum stretch ratio is two

Material	H_T/W_T(%)	H_{VE}/H_T(%)	H_P/H_T(%)	H_{VE}/W_T(%)	H_P/W_T(%)
PT-ED-30	29 %	36 %	64 %	10 %	19 %
PT-ED-20	26 %	40 %	60 %	11 %	15 %
PE-HMDA-30	47 %	29 %	71 %	14 %	33 %
PE-HMDA-20	55 %	62 %	38 %	34 %	21 %

of the materials used in this study. Second column is the total work done, W_T, on the material during loading and it is calculated by integrating the loading curve only. Third column, H_T, is total hysteresis that is the area between loading and unloading curves. Fourth column is the amount of viscoelastic work, H_{VE}, within the total hysteresis which is calculated by the derived formula. H_P is the plastic portion of hysteresis that is found by subtracting the viscoelastic amount from total hysteresis. Columns of Table 6.2 are the representations of the first four columns of Table 6.1 in percentages such that second column is the percentage of total hysteresis with respect to total work. Rest of the columns are the percentage of viscoelastic work with respect to total hysteresis, percentage of plastic portion with respect to total hysteresis, percentage of viscoelastic portion with respect to total work and percentage of plastic portion with respect to total work respectively.

As it can be seen from Table 6.1 and Table 6.2, the percentage of total hysteresis with respect to total work is much larger for PE based samples than PTMO based samples. This indicates that PE based samples have more energy absorbing capability than PTMO based ones. For PTMO based materials, the amount of hard segment within the polymer does not affect the percentage values. The values are slightly larger for the high hard segment

content PT-ED sample, but this difference is small and not very significant. On the other hand, increasing the hard segment content results in decreasing the amount of viscoelastic work in total hysteresis for PE-HMDA samples. It can be said that for PE based samples, recoverable amount of work that is done in one cycle decreases as the hard segment content increases.

Table 6.3: Results for a cycle in which the maximum stretch ratio is three

Material	W_T(Nm)	H_T(Nm)	H_{VE}(Nm)	H_P(Nm)
PT-ED-30	0.314	0.177	0.034	0.143
PT-ED-20	0.219	0.085	0.027	0.058
PE-HMDA-30	0.238	0.135	0.046	0.089
PE-HMDA-20	0.113	0.06	0.037	0.023

Table 6.4: Percentage results for a cycle in which the maximum stretch ratio is three

Material	H_T/W_T(%)	H_{VE}/H_T(%)	H_P/H_T(%)	H_{VE}/W_T(%)	H_P/W_T(%)
PT-ED-30	56 %	19 %	81 %	11 %	45 %
PT-ED-20	38 %	32 %	68 %	12 %	26 %
PE-HMDA-30	57 %	34 %	66 %	19 %	37 %
PE-HMDA-20	53 %	62 %	38 %	33 %	20 %

Table 6.3 and Table 6.4 give the same calculated values as Table 6.1 and Table 6.2, but for a cycle in which the maximum stretch ratio is 3 (elongation 200%). The percentage of total hysteresis with respect to total work increased for all materials when compared to Table 6.2. As elongation increases, the amount of energy that is absorbed by the material also increases no matter what the composition of the material is. Viscoelastic portion of total hysteresis decreased for all materials except PE-HMDA-20 for which this value stayed constant. PT-ED-30 exhibited a greater increase in the amount of plastic portion of hysteresis than its low hard segment content counterpart. It can be concluded that as hard segment content increases, the PTMO based material loses larger portion of the work done on it in cyclic loading. The same is not true for PE based samples. For PE-HMDA-30, the

viscoelastic portion of hysteresis increased when the amount of deformation is increased but it stayed constant for PE-HMDA-20.

Table 6.5: Results for a cycle in which the maximum stretch ratio is four

Material	W_T(Nm)	H_T(Nm)	H_{VE}(Nm)	H_P(Nm)
PT-ED-30	0.614	0.398	0.055	0.343
PT-ED-20	0.475	0.252	0.062	0.19
PE-HMDA-30	0.456	0.284	0.086	0.198
PE-HMDA-20	0.222	0.127	0.075	0.052

Table 6.6: Percentage results for a cycle in which the maximum stretch ratio is four

Material	H_T/W_T(%)	H_{VE}/H_T(%)	H_P/H_T(%)	H_{VE}/W_T(%)	H_P/W_T(%)
PT-ED-30	65 %	14 %	86 %	9 %	56 %
PT-ED-20	53 %	25 %	75 %	13 %	40 %
PE-HMDA-30	62 %	30 %	70 %	19 %	43 %
PE-HMDA-20	57 %	59 %	41 %	34 %	23 %

In Table 6.5 and Table 6.6, the calculated values for the same materials for a cycle in which the maximum stretch ratio is 4 (elongation 300%) is given. The amount of area between loading and unloading curves (total hysteresis) with respect to total work increased when compared to previous cycles which were explained above. For both PTMO based samples, the viscoelastic portion of hysteresis decreased. This amount is smaller in PT-ED-30 than PT-ED-20 which is consistent with the previous observations. Plastic portion of hysteresis increased up to 70% for PE-HMDA-30. Although this value did not remain constant for PE-HMDA-20 this time, it increased very slightly (from 38% to 41%). This value for the plastic portion of hysteresis is the smallest for all materials. It is interesting to note that although the elongation is 300% (which can be considered to be large), PE-HMDA-20 still exhibits mostly recoverable deformation while the other materials mostly exhibit plastic deformation.

Table 6.7: Results for a cycle in which the maximum stretch ratio is five

Material	W_T(Nm)	H_T(Nm)	H_{VE}(Nm)	H_P(Nm)
PT-ED-30	1.189	0.847	0.089	0.758
PT-ED-20	0.576	0.342	0.066	0.276
PE-HMDA-30	0.597	0.393	0.127	0.266
PE-HMDA-20	0.421	0.259	0.116	0.143

Table 6.8: Percentage results for a cycle in which the maximum stretch ratio is five

Material	H_T/W_T(%)	H_{VE}/H_T(%)	H_P/H_T(%)	H_{VE}/W_T(%)	H_P/W_T(%)
PT-ED-30	71 %	10 %	90 %	7 %	64 %
PT-ED-20	59 %	20 %	80 %	11 %	48 %
PE-HMDA-30	65 %	32 %	68 %	21 %	44 %
PE-HMDA-20	61 %	45 %	55 %	27 %	34 %

Table 6.7 and Table 6.8 give the calculated values for a cycle in which the maximum stretch ratio is 5 (elongation 400%). Total hysteresis values with respect to total work are the largest among all values that were given previously. For PTMO based samples, the trend is the same as before. The viscoelastic portion of total hysteresis decreased as deformation increased and this effect is more pronounced in the high hard segment content sample than its low hard segment content counterpart. For PE-HMDA-30, the values changed slightly which means that the amount of plastic deformation in this material did not change when elongation changed. On the other hand, PE-HMDA-20 exhibited a considerable increase in the amount of plastic portion of hysteresis (41% to 55%). This means that the amount of plastic deformation in this material increased as the elongation increased from 300% to 400%.

Figure 6.5 is the plot of total hysteresis vs percentage elongation whose values are taken from the above tables. If the results are compared with the WAXS patterns and crystallization trends given in Chapter 5, increase in total hysteresis with elongation in PTMO based samples can be attributed to the strain induced crystallization of the soft segment. This effect is more pronounced for the high hard segment content sample which showed a

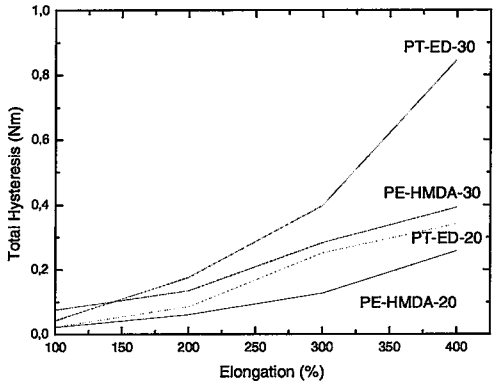

Figure 6.5: Total Hysteresis vs. Percentage Elongation for four materials

higher degree of crystallinity. For PE based samples, the increase in total hysteresis with elongation is small and it is larger for PE-HMDA-30 than PE-HMDA-20.

Figure 6.6 shows the total Hysteresis / work Total (%) vs. elongation (%) graph for four materials. The amount of total hysteresis with respect to total work done on the material for one cycle increases as elongation is increased for PTMO based samples. This increase is larger for the high hard segment content sample. For PE based samples, the increase is smaller than PTMO based ones. PE-HMDA-30 exhibits slightly larger values than its low hard segment content counterpart.

Figure 6.7 is the plot of hysteresis plastic / total hysteresis (%) vs. elongation (%) for four materials. In PTMO based samples, the plastic portion of hysteresis increases as elongation is increased. The high hard segment content sample exhibits this effect more than its low hard segment counterpart. There is not a regular trend in PE based samples. It seems as the amount of plastic portion changes very slightly as the deformation is changed in PE-HMDA-30. On the other hand, PE-HMDA-20 seems to be insensitive to changes in elongation up to 300%, but there is a considerable increase in plastic deformation after this elongation.

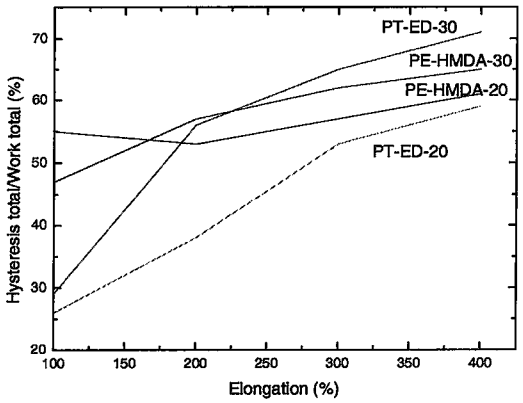

Figure 6.6: Total Hysteresis / Work Total (%) vs. Percentage Elongation for four materials

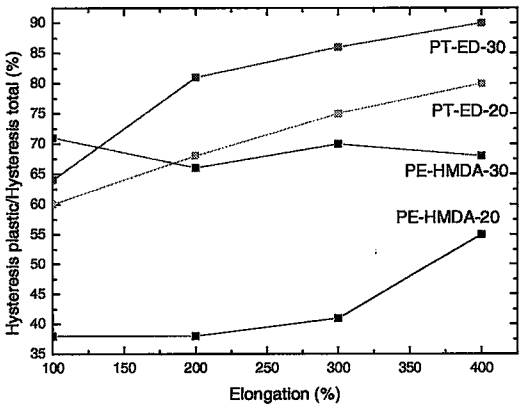

Figure 6.7: Hysteresis Plastic / Total Hysteresis (%) vs. Percentage Elongation for four materials

Chapter 7

CONCLUSION

For the experimental part, eight different samples were synthesized by selectively varying the amount and type of soft segment and hard segment. The effect of these changes on the mechano-optical properties was examined by uniaxial stretching and hysteresis experiments coupled with offline WAXS.

All of the PTMO based samples showed the two crystalline diffraction peaks at the same 2θ angle which is characteristic to PTMO. On the other hand, PEO based samples showed little or no crystallization right after stretching. But crystallinity developed over time while the samples were kept in stretched state for these materials. The samples whose chain extender was ED showed higher crystallizability no matter which soft segment was used. Hard segment concentration was found to affect both true stress-true strain values and crystallizability. Since hard segment is the part that gives strength, samples with high hard segment content showed larger true stress values than their low hard segment content counterparts. Reduction of hard segment concentration lead to improved strain crystallizabilities regardless of the material composition. Strain induced crystallization of PTMO is more pronounced as the hard segment content in the sample increases. It was interesting to see that crystallization sets in at very high true strain values for the PT-HMDA-20 sample but spreads out more on its high hard segment counterpart. The strain rate has a considerable effect on the crystallization behavior of two PTMO based materials which are in the same group. While crystallization in PT-HMDA-20 decreases with increasing strain rate, it increases for the PT-HMDA-30 sample. The birefringence-true stress curves had very small linear regions for all materials. This was attributed to presence of phase segregated structures in these materials that act as long range physical network causing the deviation from the initial linear stress optical behavior. Hysteresis was observed in all samples. As the stretch ratio increased, the amount of hysteresis also increased. When the WAXS patterns are compared for all samples, there is better crystallization at the end of hysteresis than at

the end of uniaxial stretching.

For the theoretical part, a model is proposed to calculate the amount of energy that is recoverable in hysteresis due to the viscoelastic nature of the TPUU's under consideration. The plastic portion which is permanently lost was then calculated by subtracting the viscoelastic amount from total hysteresis. The results of calculations were found to be in agreement with the results acquired during the experimental section. According to the results of these calculations, PE based samples were found to have more energy absorbing capability than PTMO based ones. For PE based samples, recoverable amount of work that is done in one cycle decreases as the hard segment content increases. When the maximum elongation for the cycle was increased, the amount of energy that is absorbed by the material also increased no matter what the composition of the material was. The largest increase in total hysteresis with elongation belongs to PT-ED-20 sample, which was found to be the most easily crystallizable sample among others. If the results are compared with the WAXS patterns and crystallization trends given in the experimental part, the increase in total hysteresis with elongation in PTMO based samples can be attributed to the strain induced crystallization of the soft segment. This effect is more pronounced for the high hard segment content sample which showed a high degree of crystallinity. In PTMO based samples, the plastic portion of hysteresis increases as elongation is increased. The high hard segment content sample exhibits this effect more than its low hard segment counterpart. On the other hand, PE based samples seem to be insensitive to changes in elongation up to 300%. After this point, while there is a considerable increase in plastic deformation for PE-HMDA-20, there is still a very slight change for PE-HMDA-30.

BIBLIOGRAPHY

[1] SL Cooper AV Tobolsky, "Properties of linear elastomeric polyurethans," *Journal of Applied Polymer Science*, vol. 10, pp. 1837–1844, 1966.

[2] NS Schneider SB Clough, ," *Journal of Macromolecular Sci. Phys.*, vol. B2, pp. 553–566, 1968.

[3] AO King SB Clough, NS Schneider, ," *Journal of Macromolecular Sci. Phys.*, vol. B2, pp. 641–648, 1968.

[4] R Bonart, "X-ray investigations concerning the physical structure of cross-linking in segmented urethane elastomers," *Journal of Macromolecular Sci. Phys.*, vol. B2, pp. 115–138, 1968.

[5] GL Wilkes YJP Chang, "Superstructure in segmented polyether-urethanes," *Journal of Polymer Sci. Phys.*, vol. 13, pp. 455–476, 1975.

[6] SL Cooper GM Estes, RW Seymour, "Infrared studies of segmented polyurethane elastomers. II. infrared dichroism," *Macromolecules*, vol. 4, pp. 452–457, 1971.

[7] ED Muller R Bonart, L Mobitzer, "X-ray investigations concerning the physical structure of crosslinking in urethane elastomers. III. common structure principles for extensions with aliphatic diamines and diols," *Journal of Macromolecular Sci. Phys.*, vol. 9, pp. 447–461, 1974.

[8] CS Yusek CE Wilkes, "Investigation of domain structure in urethane elastomers by x-ray and thermal methods," *Journal of Macromolecular Sci. Phys.*, vol. B7, pp. 157–175, 1973.

[9] TW Smith CSP Sung, NH Sung, "Properties of segmented polyether poly(urethaneureas) based on 2,4-toluene diisocyanate. 2. infrared and mechanical studies," *Macromolecules*, vol. 13, pp. 117–121, 1980.

[10] CS Wu CSP Sung, CB Hu, "Properties of segmented poly(urethaneureas) based on 2,4-toluene diisocyanate. 1. thermal transitions, x-ray studies, and comparison with segmented poly(urethanes)," *Macromolecules*, vol. 13, pp. 111–116, 1980.

[11] CB Hu CSP Sung, "Orientation studies of segmented polyether poly(urethaneurea) elastomers by infrared dichroism," *Macromolecules*, vol. 14, pp. 212–215, 1981.

[12] S Abouzahr GL Wilkes, "SAXS studies of segmented polyether poly(urethaneurea) elastomers," *Macromolecules*, vol. 14, pp. 456–458, 1981.

[13] CB Wang SL Cooper, "Morphology and properties of segmented polyether polyurethaneureas," *Macromolecules*, vol. 16, pp. 775–786, 1983.

[14] RW Seymour AE Allegrezza, SL Cooper, "Segmental orientation studies of block polymers. i. hydrogen-bonded polyurethanes," *Macromolecules*, vol. 6, pp. 896–902, 1973.

[15] H Ono N Yoshihara S Nomura H Kawai I Kimura, H Ishihara, "Morphology and deformation mechanism of segmented poly(urethaneureas) in relation to spherulitic crystalline textures," *Macromolecules*, vol. 7, pp. 355–363, 1974.

[16] K Saito H Ono H Ishihara, I Kimura, ," *Journal of Macromolecular Sci. Phys.*, vol. B10, pp. 591, 1974.

[17] NS Schneider B Fu, WJ Macknight, "Structure-property relationships of segmented polyurethanes containing monodisperse 2,4-toluene diisocyanate/butanediol hard segments," *Rubber Chem. Tech.*, vol. 59, pp. 896–911, 1986.

[18] D Yang SL Hsu CW Meuse, X Yang, "Spectroscopic analysis of ordering and phase-separation behavior of model polyurethanes in a restricted geometry," *Macromolecules*, vol. 25, pp. 925–926, 1992.

[19] LM Leung JT Koberstein, AF Galambos, "Compression-molded polyurethane block copolymers. 1. microdomain morphology and thermomechanical properties," *Macromolecules*, vol. 25, pp. 6195–6204, 1992.

[20] NH Ny HN Cooper AE Allegrezza, RW Seymour, "Segmental orientation studies of block copolymers: 2. non-hydrogen bonded polyurethanes," *Polymer*, vol. 15, pp. 433–440, 1974.

[21] JE McGrath A. Noshay, *Block Copolymers-An Overview and Critical Survey*, Academic„ New York, 1977.

[22] Eastman Kodak Co, "British patent 1.118.731," June 1964.

[23] LL Harrell, "Segmented polyurethanes. properties as a function of segment size and distribution," *Macromolecules*, vol. 2, pp. 607–612, 1969.

[24] GL Wilkes S Abouzahr, *Processing Structure and Properties of Block Copolymers*, M.J. Folkes, ed., Elsevier, London, 1985.

[25] SB Lin SY Tsay SL Cooper, KS Hwang, "Segmental orientation studies of polyether polyurethane block copolymers with different hard segment lengths and distributions," *Colloid and Polymer Science*, vol. 263, pp. 128–140, 1985.

[26] JS Lin NS Schneider CR Desper, JP Jasinski, "Deformation of microphase structures in segmented polyurethanes," *Macromolecules*, vol. 18, pp. 2755–2761, 1985.

[27] M Morton, ," *Encyclopedia of Polymer Science Technology*, vol. 11, pp. 508, 1964.

[28] TC Ward JN Gorce, JW Hellgeth, "Mechanical hysteresis of a polyether polyurethane thermoplastic elastomer," *Polymer Engineering And Science*, vol. 33, pp. 1170–1176, 1993.

[29] RW Truss RA Beck, "Effect of curative and stoichiometry on the hysteresis in polyurethane-ureas," *Journal of Applied Polymer Science*, vol. 71, pp. 959–966, 1999.

[30] JT Koberstein LM Leung, "DSC annealing study of microphase separation and multiple endothermic behavior in polyether-based polyurethane block copolymers," *Macromolecules*, vol. 19, pp. 706–713, 1986.

[31] A Sadijarevic V Sadirajewic KC Frisch EG Bajsic, V Rek, ," *Journal of Elastomers Plast.*, vol. 32, pp. 162, 2000.

[32] B Helgee K Gisselfaelt, "Effect of soft segment length and chain extender structure on phase separation and morphology in poly(urethane urea)s," *Macromolecular Materials Engineering*, vol. 288, pp. 265–271, 2003.

[33] J Cho J Runt JT Garrett, R Xu, "Phase separation of diamine chain-extended poly(urethane) copolymers: FTIR spectroscopy and phase transitions," *Journal of Polymer*, vol. 44, pp. 2711–2719, 2003.

[34] K Onaran WN Findley, SL James, *Creep and Relaxation of Nonlinear Viscoelastic Materials*, Dover Publications Inc., New York, 1989.

[35] AR Payne, "Hysteresis in rubber vulcanizates," *J. Polymer Sci.:Symposium*, vol. 48, pp. 169–196, 1974.

[36] *A Pseudo-Elastic Model for Mullins Effect in Filled Rubber*, London Ser. A 455. Proc. Roy. Soc, 1999.

[37] C Miehe, "Discontinuous and continuous damage evolution in ogden-type large-strain elastic material," *Eur. J. Mech. A Solids*, vol. 14, pp. 697–720, 1995.

[38] L Teresi A DeSimone, JJ Marigo, "A damage mechanics approach to stress softening and its application to rubber," *Eur. J. Mech. A/Solids*, vol. 20, pp. 873–892, 2001.

[39] Z Carriere H Bouasse, "Courbes de traction du caouthouc vulcanize," *Annales de la des Sciences*, vol. 5, pp. 257–283, 1903.

[40] L Mullins, "Effect of stretching on the properties of rubber," *Journal of Rubber Research*, vol. 16, pp. 275–289, 1947.

[41] S Krishnaswamy MF Beatty, "A theory of stress softening in incompressible isotropic materials," *J. Mech. Phys. Solids*, vol. 48, pp. 1932–1965, 2000.

[42] NR Tobin L Mullins, "Theoretical model for the elastic behavior of filled-reinforced vulcanized rubbers," Proc. 3rd Rubber Technol. Conf, 1954, pp. 397–412, Heffer and Sons, London.

[43] JB Donnet A Vidal, "Carbon black: Surface properties and interactions with elastomers," *Advanced Polymer Science*, vol. 76, pp. 104–106, 1996.

[44] A Burr, "Continuum description of damage in ceramic-matrix composites," *Eur. J.Mech. A Solids*, vol. 1, pp. 53–78, 1997.

[45] A Dragon D Halm, "An isotropic model of damage and frictional sliding for brittle materials," *Eur. J. Mech. A Solids*, vol. 3, pp. 439–460, 1998.

[46] R Desmorat S Cantournet, "Thermodynamics modeling of internal friction and hysteresis of elastomers," *C.R. Mecanique*, vol. 331, pp. 265–270, 2003.

[47] TZ Sen B Yalcin M Cakmak D Valladares, S Toki, "The effect of natural rubber crosslink density on real time birefringence, true stress and true strain behavior," *Macromol Symp*, vol. 185, pp. 149–166, 2002.

[48] A Posthuma de Boer F Beekmans, "Determination of orientation in thermotropic liquid crystalline polymer films by spectrographic measurement of the birefringence," *Macromolecules*, vol. 29, pp. 8726–8733, 1996.

[49] A Seeger, *Handbuch der Physik*, 1958.

[50] A Seeger, *Naturforsch*, 1954.

[51] K Dinbergs CS Schollenberger, "Thermoplastic polyurethane elastomer molecular weight-property relations, further studies," *Advanced Urethane Sci. Technology*, vol. 7, pp. 1–34, 1979.

[52] NS Schneider CB Hu, RS Ward, "A new criterion of phase separation: The effect of diamine chain extenders on the properties of polyurethaneureas," *Journal of Applied Polymer Science*, vol. 27, pp. 2167–2177, 1982.

[53] LE Nielsen, "Morphology and the elastic modulus of block polymers and polyblends," *Rheol. Acta.*, vol. 13, pp. 594–600, 1974.

[54] SL Aggarwal, *Block Polymers*, Plenum Press NY, 1970.

[55] BB Sauer S Michel HW Siesler F Yeh, BS Hsiao, "In-situ studies of structure development during deformation of segmented poly(urethane-urea) elastomer," *Macromolecules*, vol. 36, pp. 1940–1954, 2003.

[56] A Kloczkowski JE Mark I Bahar, B Erman, "Lattice model for segmental orientation in deformed polymeric networks. 1. contribution of intermolecular correlations," *Macromolecules*, vol. 23, pp. 5335–5341, 1990.

[57] PJ Flory, *Statistical Mechanics of Chain Molecules*, Wiley, New York, 1969.

[58] UW Suter WL Mattice, *Conformational Theory of Large Molecules. The Rotational Isomeric State Model in Macromolecular Systems*, John Wiley and Sons Inc., New York, 1994.

VITA

SEZEN CÜRGÜL was born in Sakarya, Turkey on September 28,1979. She received her B.Sc. degree in Mechanical Engineering from Bogazici University, Istanbul, in 2002. From September 2002 to June 2004, she worked as a teaching and research assistant at the Department of Mechanical Engineering of Koc University, Turkey. She studied for the "Experimental and Theoretical Studies On The Mechano-optical Behavior of Thermoplastic Polyurethaneureas" project whose travel funds were sponsored by National Science Foundation. As a part of this project, she worked as a visiting scientist at the Polymer Engineering Department of University of Akron, Ohio.